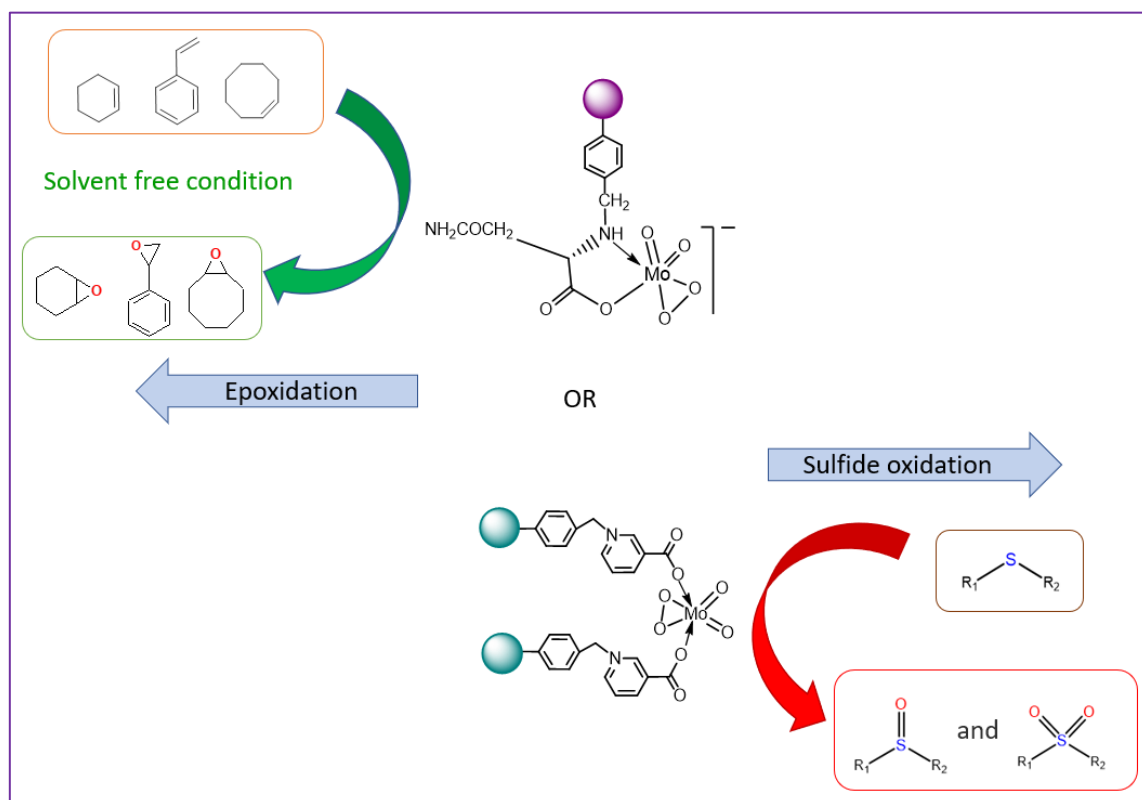# CHAPTER 5

New peroxidomolybdenum(VI) complexes immobilized on Merrifield resin: highly efficient catalysts for selective oxidation of sulfides and olefins under solvent-free condition

5.1 Introduction

The epoxidation of alkenes is a highly important industrial transformation in organic synthesis as epoxides are precious building blocks in the synthesis of a diverse range of fine and bulk chemicals [1-5]. As revealed by a survey of literature, dioxidomolybdenum(VI) complexes are among the most active epoxidation catalysts [6-7]. However, majority of these methodologies, typically utilize expensive, non-aqueous organohydroperoxides such as tert-butyl hydroperoxide (TBHP) as oxygen source along with hazardous chlorinated solvents to achieve high activity [8-16]. Such limitations are becoming more conspicuous in view of the current intense search for new oxidation methodologies that are not only efficient, selective and high yielding, but are also ecologically benign. Use of greener oxidants and solvent-free conditions are emerging as key issues in green synthetic strategy. Moreover, development of synthetic methodologies which promote the use of active as well as recyclable heterogeneous catalysts has long been a challenge in organic chemistry. Solvent-free organic transformations being cost efficient and environmentally safe are economically and industrially useful as such systems contribute considerably towards waste minimization [17]. On the other hand, aqueous hydrogen peroxide with high oxygen content offers a predominantly desirable choice of green oxidant as it is readily available, inexpensive, safe, and generates water as the only by product [18-20].

Notwithstanding the numerous innovative and promising oxidoperoxido Mo(VI) complexes based homogeneous and heterogeneous catalysts reported for olefin epoxidation in the past decades, there is still a dearth of information on pMo catalyzed olefin epoxidation under solvent free condition [6,21]. Recently Zara *et al.* reported a pMo based heterogeneous catalyst for the olefin epoxidation using TBHP as oxidant under solvent free condition at 95 ^{0}C [22]. With H_2O_2 as an oxidant, Herbert and co-workers carried out epoxidation of cyclooctene using soluble peroxidomolybdenum catalyst containing pyridine or pyrazole ligands under solvent-free condition [23]. However, the reaction required base additives and a temperature of 60 ^{0}C. Moreover, the system was not effective for epoxidation of other olefinic substrates and catalyst regeneration was an issue.

Merrifield resin (**MR**) or cross-linked poly(styrene-divenylbenzene) with its potential to undergo facile functionalization still stand out as one of the most attractive

macromolecular supports for catalytic applications [24-25]. Previously, our group has developed highly efficient heterogeneous catalysts by grafting pMo or peroxidotantalum species on to functionalized MR, which exhibited excellent activity in selective oxidation of sulfides to the corresponding sulfoxide and sulfone by H_2O_2 under mild condition [26-27]. Moreover, the same MR-peroxidotantalum complexes served as active catalysts for epoxidation of variety of olefins with H_2O_2 in absence of solvent.

These exciting results provided us with the impetus to direct our efforts to develop new versatile **pMo** based heterogeneous catalysts supported on appropriately functionalized MR. Since the catalytic activity and selectivity of such functionalized systems mainly depend on the coordination sphere created by the chelating ligands, proper choice of functional group is an essential requirement in order to obtain the metal supported catalyst that should be catalytically active and robust during the reaction and recycling process.

This chapter describes the development of a pair of new heterogeneous **pMo** catalysts supported on **MR** functionalized with ligands L-asparagine or nicotinic acid and their role as recoverable heterogeneous catalysts in olefin epoxidation as well as sulfide oxidation with H_2O_2 under mild condition. Asparagine (**Asn**), a bulky tridentate amino acid ligand with polar side chains offers excellent coordination facility in the formation of various stable metal complexes [28-32]. Nicotinic acid (niacin) or pyridine-3-carboxylic acid which contains carboxyl ligating group forms different types of metal complexes that are used as therapeutic agents [33-39]. This biological ligand may present in the complex in neutral, anionic or zwitterionic form. To the best of our knowledge, these ligands have not been used so far for attaching pMo species to **MR**.

5.2 Experimental section

5.2.1 Functionalization of the Merrifield resin (MR):

In this work, functionalization of the polymer support with the ligands was achieved according to the methods reported earlier with some modifications [26-27,40-41]. 2 g (5 mmol Cl) of pre-washed chloromethylated poly(styrene-divinylbenzene) copolymer beads were swelled in 6 mL methanol for 1 h at room temperature. An aqueous solution of L-asparagine (0.82 g, 6.25 mmol) or nicotinic acid (0.76 g, 6.25 mmol) in 20 mL distilled water was added to the swollen polymer in methanol. The molar ratio

of Cl:ligand:base on the basis of percent replaceable chlorine on resin was maintained approximately at 1:1.25:1.25. The resulting system was then kept for 24 h under refluxing conditionin presence of pyridine (0.50 mL, 6.25 mmol). The contents were cooled and allowed to stand at room temperature for a week with occasional shaking. After 7 days, pH of the reaction mixture containing L-asparagine decreased to *ca*. 5 from its initial value *ca*. 7, while for the system containing nicotinic acid, pH was observed *ca.* 3.5 from its initial value 5.2. The color of the beads were observed to change from off-white to pale yellow indicating the attachment of the ligand. Finally, the L-asparagine or nicotinic acid functionalized polymer beads were collected by filtration, followed by washing with hot water till no precipitate of AgCl was observed in the filtrate on treating with $AgNO_3$. It was further rinsed with excess ethanol. The final product was obtained after drying at 90 ^{0}C in an oven for 6 h to yield 2.65 g of **MRAsn** and 2.51 g of **MRNA** respectively.

5.2.2 Synthesis of immobilized molybdenum dioxidomonoperoxido compounds $[MoO_2(O_2)(L)]^-$—MR, [L = Asparagine (MRAsnMo) (5.1)] or $[MoO_2(O_2)(L)_2]$—MR, [L = Nicotinic acid (MRNAMo) (5.2)]

Molybdic acid (0.40 g, 2.5 mmol) was dissolved in 30% H_2O_2 (2.55 mL, 22.5 mmol) at room temperature. The initial pH of the clear solution was recorded to be *ca.* 1. Sodium hydroxide solution (8 M) was then added to the above system dropwise with constant stirring until the pH of the reaction medium become 5.0. The temperature of the system was maintained below 4 ^{0}C in an ice bath. 1.0 g of **MRAsn** or **MRNA,** pre-swelled in 5 mL ethanol for 1 h was added to it. The mixture was kept for 24 h under stirring in an ice bath. The supernatant liquid of reaction mixture was decanted and the yellowish residue was repeatedly washed with pre-cooled acetone. The final products were separated by centrifugation and dried in *vacuo* over concentrated sulfuric acid.

5.2.3 Elemental analysis

Quantitative determination of molybdenum, peroxide, carbon, hydrogen, nitrogen, chlorine and sodium were obtained by the methods described in Chapter 2. The analytical data of the compounds are summarized in **Table 5.1**.

5.2.4 Physical and spectroscopic measurements

According to the methods described in Chapter 2, the compounds were characterized with the help of spectroscopic measurements, TG analysis as well as scanning electron micrographs (SEM) and EDX analysis. Structurally significant IR bands and their assignments are summarized in **Table 5.4**. TGA data of the complexes are reported in **Table 5.6**. **Table 5.5** describe the ^{13}C NMR chemical shift values for the complexes and their respective free polymers.

5.2.5 General procedure for epoxidation of alkenes

Catalytic oxidation of alkene was carried out as follows: Initially, 5 mmol of styrene and 0.005 mmol of catalyst [**MRAsnMo** (3.5 mg) or **MRNAMo** (8.3 mg)] was placed in a round bottom flask. To this 30% H_2O_2 (5 mmol, 0.56 mL) was added and the system was placed at 80 ^{0}C under continuous stirring. The molar ratio of Mo: substrate: oxidant was maintained at 1:1000:1000. The progress of the reaction was monitored by HPLC. After completion of the reaction, the solid catalyst was separated by filtering the reaction mixture and washed with acetone for further use.

The quantitative analysis of styrene and its oxidized products was performed on a Thermo-Scientific Dionex Ultimate 3000 HPLC system equipped with a UV detector. The products were detected at a wavelength of 254 nm and well separated by the use of a reversed phase C18 column (250 × 4.6 mm). The mobile phase was composed of acetonitrile, methanol and water in a volume ratio of 2:3:5 with a flow rate of 1 mL/min and an injection volume of 20 μL. The substrate and products were identified by using authentic samples. The content of the compounds in the sample was determined directly from interpolation of the calibration curves taken (**Appendix III**).

5.2.6 General procedure for oxidation of sulfide to sulfoxide

In a representative procedure, 5 mmol of substrate was added to a system containing catalyst (0.0017 mmol) [**MRAsnMo** (1.2 mg) or **MRNAMo** (2.8 mg)] in 5 mL MeOH. 10 mmol 30% H_2O_2 (1.13 mL) was then added to the above reaction mixture maintaining a Mo: substrate molar ratio of 1:3000 and a substrate: H_2O_2 molar ratio of 1:2 in a 50 mL two necked round-bottomed flask. The reaction was conducted at room temperature under continuous stirring. The progress of the reaction was monitored by thin-layer chromatography (TLC) and GC. After completion of the reaction, the catalyst

was removed from the system by filtration and washed with profuse amount of acetone. The products and unreacted substrates were extracted with diethyl ether. The corresponding sulfoxide obtained was purified by column chromatography on silica gel using ethyl acetate and n-hexane (1:9). The products obtained were characterized by IR, ^{1}H NMR and ^{13}C NMR spectroscopy, and in case of solid products, in addition to the above analysis, we have also carried out melting point determination (**Appendix I**).

5.2.7 General procedure for oxidation of sulfide to sulfone

In a typical reaction, 0.005 mmol of catalyst [**MRAsnMo** (3.5 mg) or **MRNAMo** (8.3 mg)] was added to 5 mmol of sulfide followed by the addition of 15 mmol 50% H_2O_2 (1.02 mL) in a 50 mL two necked round-bottomed flask. The molar ratio of substrate: H_2O_2 and that of catalyst (Mo): substrate was maintained at 1:3 and 1:1000, respectively. The reaction was conducted at room temperature under magnetic stirring. The reaction progress was monitored by thin layer chromatography (TLC) and GC. After completion, the product and unreacted organic substrates were extracted with diethyl ether, over anhydrous sodium sulfate and distilled under reduced pressure to remove excess solvent. The crude product obtained was purified by column chromatography on silica gel with ethyl acetate-hexane (1:9 v/v) as the eluent. The product obtained was characterized by a combination of IR, ^{1}H NMR, ^{13}C NMR spectroscopy and melting point determination (**Appendix II**).

5.2.8 Regeneration of the catalyst

Regeneration and recyclability of the catalysts were examined using styrene as the substrate for epoxidation reaction. After completion of the reaction (as mentioned under **Section 5.2.5**), the catalyst was separated from the reaction mixture by filtration, washed with excess amount of acetone and dried in *vacuo*. The recovered solid catalyst was then added to a fresh reaction mixture of styrene (5 mmol) and 30% H_2O_2 (5 mmol) to repeat the experiment under the optimized reaction condition. The progress of the reaction was monitored by HPLC.

In case of oxidation of sulfide to either sulfoxide or sulfone, the solid catalyst was similarly recovered and the dried catalyst was then reused in subsequent cycles of oxidation. The oxidation reactions were repeated up to ten reaction cycles for each catalyst in the production of sulfoxide under optimized condition (**Section 5.2.6**). In

sulfide to sulfone oxidation, the process was repeated for six cycles of reaction under standard condition as mentioned in **Section 5.2.7**.

5.3 Results and discussion

5.3.1 Synthesis

The preparation of polymer immobilized catalysts, **MRAsnMo** (**5.1**) and **MRNAMo** (**5.2**) involved a two steps synthetic protocol, as depicted in **Scheme 5.1**. Chloromethylated polystyrene cross-linked with 2% DVB was used as support mainly due to its superior flexibility, which is known to facilitate grafting of metallic atoms *via* polymer anchored ligands [26-27,42-43]. To obtain the catalyst **5.1**, the polymer resin was functionalized in the first step with L-asparagine using pyridine as base according to the previously established procedure [26-27,40]. The niacin grafted resin **MRNA**, was isolated in a similar manner by using niacin in lieu of L-asparagine [26-27,40-41]. Reaction of the respective functionalized polymer with **pMo** species, generated *in situ* by reacting H_2MoO_4 with 30% H_2O_2, afforded the catalysts **5.1** and **5.2.**
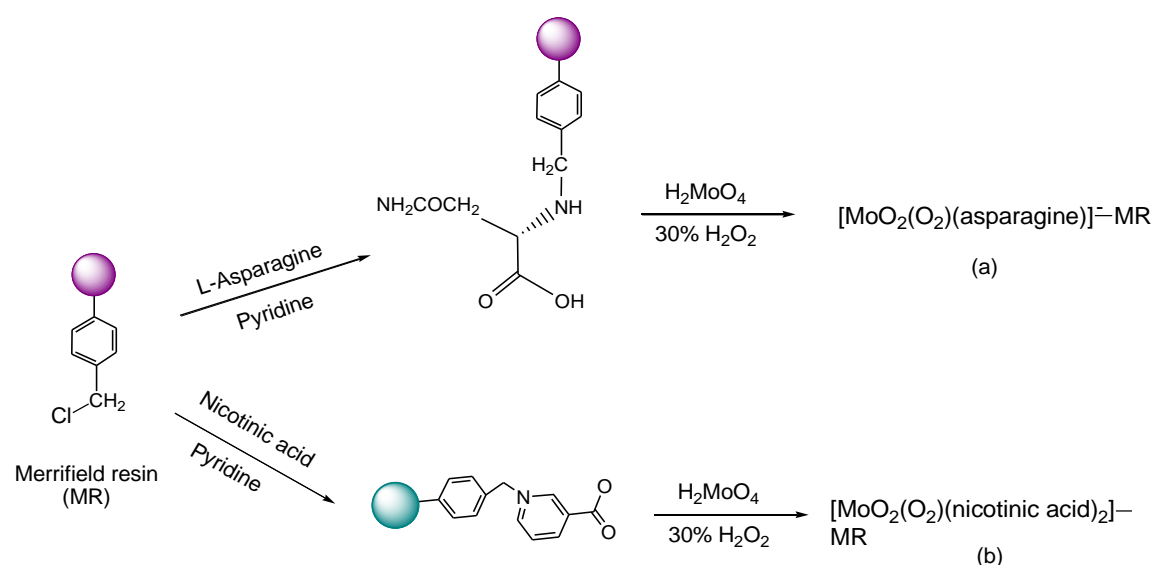
Scheme 5.1 Synthesis of chloromethylated poly(styrene divinylbenzene) supported **pMo** complexes, (a) $[MoO_2(O_2)(L)]^-$—MR, (L = L-Asparagine) (**MRAsnMo**) and (b) $[MoO_2(O_2)(L)_2]$— MR, (L = Nicotinic acid) (**MRNAMo**). " ⬤ " represents polymer chain.

Maintenance of pH of the reaction mixture at *ca*. 5 was found to be optimal for the formation and subsequent isolation of each of the catalysts. It is significant to note that these catalysts, unlike many of the reported monomeric peroxidometallates, were found to be non-hygroscopic and stable for a prolonged period without any alteration in its catalytic efficiency.

5.3.2 Characterization and formulation

The elemental analysis data for the synthesized compounds in each step of synthesis are presented in **Table 5.1**. From the elemental analysis it was observed that complete removal of the Cl of -CH$_2$Cl groups by L-asparagine took place during the functionalization to form **MRAsn**. Whereas, almost 87% of Cl was replaced by the nicotinic acid (**NA**) to form **MRNA**. The occurrence of the **pMo** species in the complexes in their monoperoxido form was indicated by the ratio of Mo:O$_2^{2-}$ content which was found to be nearly unity. The molybdenum loading on the compounds, **MRAsnMo** (**5.1**) and **MRNAMo** (**5.2**) correspond to 1.41 and 0.60 mmol per gram of the polymeric support, respectively which was calculated on the basis of Mo content, obtained from elemental analysis and confirmed by EDX spectral analysis as well as with inductively coupled plasma optical emission spectrometry (ICP-OES). The **pMo** compounds were diamagnetic in nature, in conformity with the presence of Mo centers in their +6 oxidation states which was further confirmed from XPS analysis data.

5.3.2.1 SEM and Energy Dispersive X-ray (EDX) Analysis

The surface morphology of the synthesized peroxidomolybdenum (**pMo**) complexes were studied at different stages of preparation and are shown in **Fig. 5.1**. The SEM images revealed that the smooth surface of the starting resin, **MR** [**Fig. 5.1(a)**] undergoes considerable roughening upon functionalization with the ligands [**Fig. 5.1(b)** and **5.1(e)**]. Further roughening was observed along with randomly oriented depositions on the surfaces of the polymeric catalysts **MRAsnMo (5.1)** and **MRNAMo (5.2)** after incorporation of **pMo** units [**Fig. 5.1(c)**-(**d**) and **5.1(e)**-(**f**)].

Table 5.1 Analytical data for the functionalized Merrifield resin and polymer-bound peroxidomolybdates

Compound	% Found from elemental analysis (% obtained from EDX spectra)							Molybdenum loading [a] (mmol g^{-1} of polymer)
	C	H	N	Cl	Na	Mo	O_2^{2-}	
MRAsn	73.06	6.96	7.11	--	--	--	--	
	(77.74)	--	(6.97)	--	--	--	--	
MRNA	80.56	7.70	3.39	--	--	--	--	
	(75.81)	--	(3.34)	(0.94)	--	--	--	
MRAsnMo	56.49	5.80	6.71	--	2.61[b]	13.38	4.68	1.41
	(55.54)	--	(6.49)	--	(2.83)	(13.63)	--	
MRNAMo	70.82	6.50	2.96	--	--	5.81	2.1	0.60
	(68.32)	--	(3.03)	(0.86)	--	(5.84)	--	

[a] Molybdenum loading = $\dfrac{\text{Observed metal \% X 10}}{\text{Atomic weight of metal}}$

[b] Determined by ICP-OES.
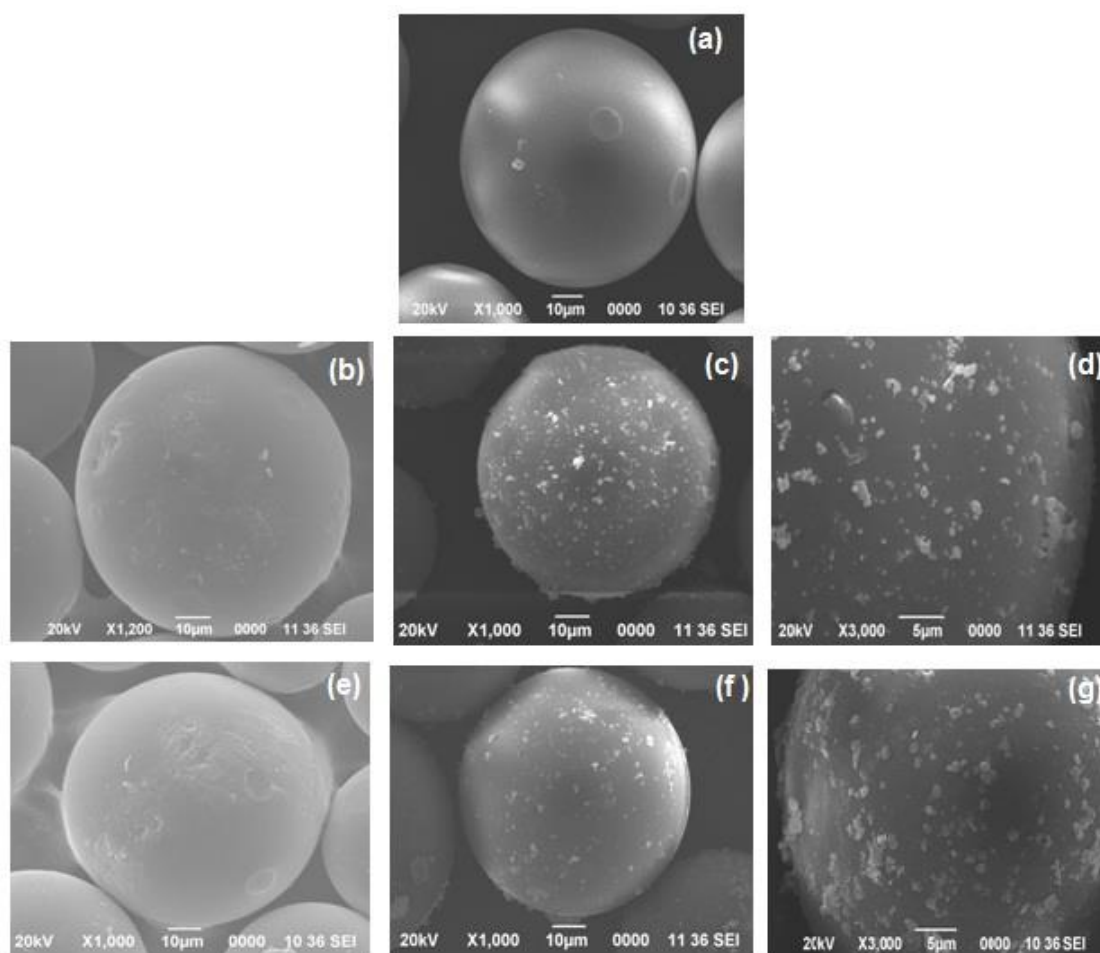
Fig. 5.1 Scanning electron micrographs of (a) **MR**, (b) **MRAsn**, (c) **MRAsnMo** at 10 µm, (d) **MRAsnMo** at 5µm, (e) **MRNA**, (f) **MRNAMo** at 10 µm and (g) **MRNAMo** at 5 µm.

Successful functionalization of the resin and subsequent formation of the **pMo** immobilized compounds were also evident from the energy dispersive X-ray spectroscopic analysis, that was carried out focusing multiple regions over the surface of the polymer at different stages of synthesis. EDX spectra showed Mo, C, N and O as the constituents of the compounds **5.1** and **5.2**) (**Fig. 5.2**). The EDX analysis also confirms the presence of sodium as the counter ion in **MRAsnMo**. The composition of the compounds as obtained by EDX analysis is in close agreement with the elemental analysis values as shown in **Table 5.1**.
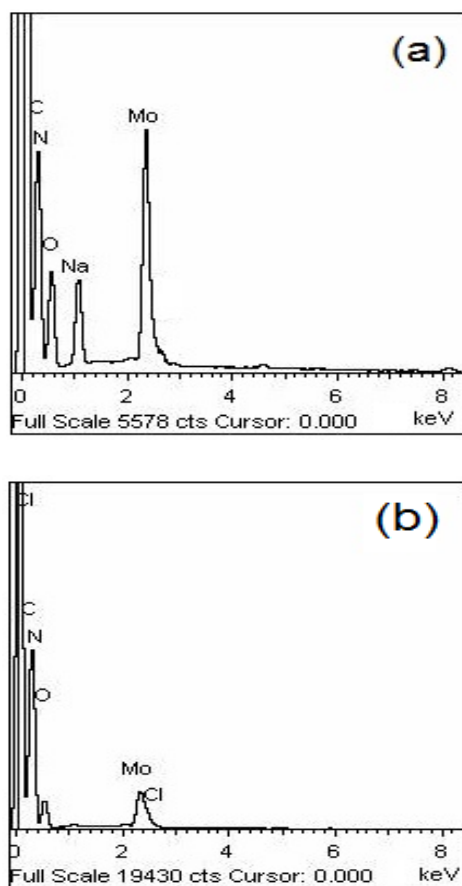
Fig. 5.2 EDX spectra of (a) **MRAsnMo** and (b) **MRNAMo**.

5.3.2.2 Powder X-ray diffraction (XRD) studies

The crystal phase analysis of the systhesized peroxido molybdenum complexes (**MRAsnMo** and **MRNAMo**), functionalized resins (**MRAsn** and **MRNA**) as well as the pristin polymer (**MR**) has been performed under the range of $10 \leq 2\theta \leq 70^0$ and are shown in **Fig. 5.3**. The XRD spectrum reveals that each of the samples contains a broad peak at 2θ value of 20° which is the charecteristic diffraction pattern for PS-DVB resin [44-45]. This shows that during the systhesis of the polymer supported peroxido Mo(VI) complexes, the amorphous nature of **MR** remains unchanged. For the functionalized resins (**MRAsn** or **MRNA**), no change in the diffraction pattern was observed compared to the pristin polymer **MR**. In contrast, both the complexes **MRAsnMo** and **MRNAMo** exhibited some new peaks at 2θ values of 14.62, 15.64, 26.49^0 and 14.65, 15.69, 26.49^0 respectively. These peak values were found close to the main crystalline peaks observed for the monoperoxidomolybdate species with the corresponding phases at (200), (101) and (011) respectively (PDF 41-359), thus confirming the presence of monoperoxido
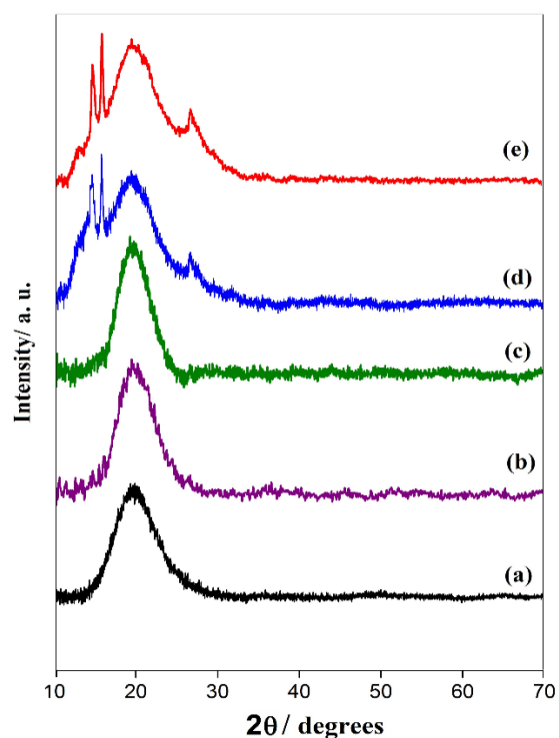
Fig. 5.3 X-ray diffraction (XRD) pattern of (a) **MR**, (b) **MRNA**, (c) **MRAsn**, (d) **MRNAMo** and (e) **MRAsnMo**.

molybdate moeity in the synthesized complexes. No additional peak was observed in any stage of the samples during the synthesis and this shows high purity of the synthesized compounds.

5.3.2.3 X-ray photoelectron spectroscopy

XPS investigation was further performed to identify the possible oxidation state of the molybdenum ions present on the surface of the catalysts. The XPS spectra of Mo(3d) core for the complexes are shown in **Fig. 5.4**. **Table 5.2** displays the experimental values obtained for complexes **MRAsnMo** and **MRNAMo**. The analysis data revealed that the surface bound Mo ions in both the complexes are in +6 oxidation state [46-48]. For the complex **MRAsnMo**, the binding energy for Mo(3d) core was observed at a higher value in comparison to the Mo(3d) binding energy for **MRNAMo**. This variation further indicates that in the two complexes the metal is in different coordination environment. The XPS analysis results were found to be in agreement with the magnetic susceptibility measurements which show diamagnetic nature of the complexes.

Table 5.2 Mo(3d) binding energies of the complexes **MRAsnMo** and **MRNAMo**

Compounds	Binding energy (eV)	
	$3d_{3/2}$	$3d_{5/2}$
MRAsnMo	233.4	236.4
MRNAMo	232.5	235.6
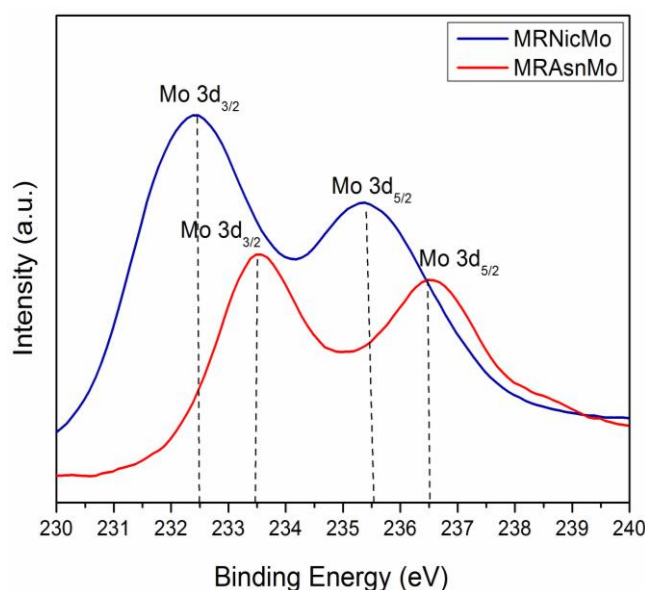
Fig. 5.4 XPS core level spectra for Mo ($3d_{3/2}$) and Mo ($3d_{5/2}$) for **MRAsnMo** and **MRNAMo**.

5.3.2.4 BET analysis

The surface area of the polymeric samples was measured by using BET analysis with the nitrogen adsorption method [49] and pore volume was determined by BJH model [50]. The experimental data presented in **Table 5.3** reveal that a significant decrease in the surface area, total pore volume and pore radius occur after functionalization of the virgin polymer **MR.** Further treatment of the functionalized resins (**MRAsn** or **MRNA**) with **pMo** species resulted in more reduced values in the compounds **MRAsnMo** (**5.1**) or **MRNAMo** (**5.2**). The lowering of BET parameters is presumably due to blocking of pores because of functionalization and incorporation of peroxidomolybdenum moieties [26-27]. The N_2 adsorption/desorption isotherms for each

of the samples showed typical TYPE II adsorption of an IUPAC standard on particles which have macropores or nonpores, showing poor adsorption (**Fig. 5.5**) [51-53].

Table 5.3 BET surface area, V_{tot} and pore radius of the **pMo** compounds **5.1** and **5.2** and base polymers

Compound	S_{BET}^{a} (m^2/g)	V_{tot}^{b} (cc/g)	Pore radius (Å)
MR	11.4	0.12	53.7
MRAsn	9.6	0.10	39.9
MRNA	5.3	0.05	17.9
MRAsnMo	8.7	0.09	36.1
MRNAMo	2.5	0.03	15.1

[a] BET surface area.
[b] Total pore volume.
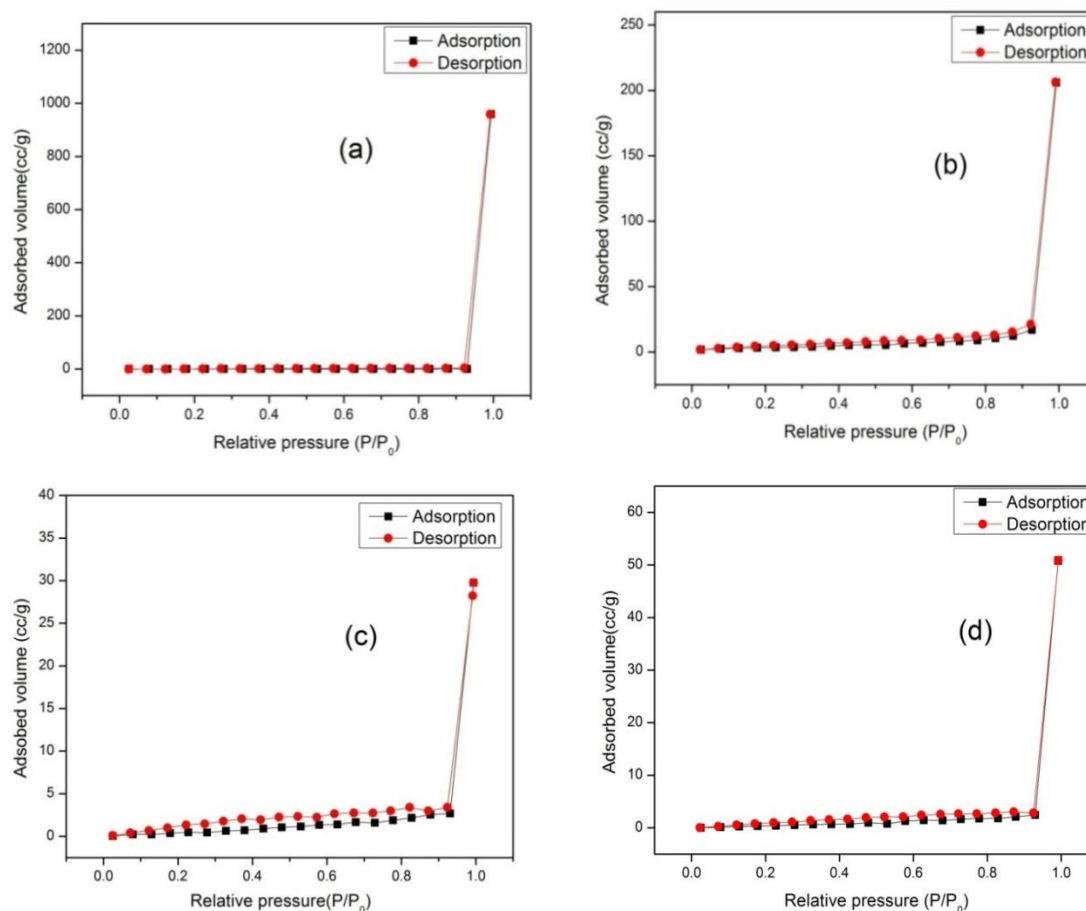
Fig. 5.5 The N_2 adsorption/desorption isotherm of (a) **MRAsn**. (b) **MRAsnMo**, (c) **MRNA** and (d) **MRNAMo**.

5.3.2.5 IR and Raman spectral studies

FTIR spectra of the compounds were recorded at each step of synthesis and are shown in **Fig. 5.6** and **Fig. 5.7**. Characteristic differences in the IR spectrum of the pristine polymer, the functionalized resins and the polymer-metal complexes either by shifting of peaks or by appearance of new bands were observed. Important peaks were assigned on the basis of available literature (**Table 5.4**) [26-27,40,54-57]. In the spectrum of complexes **MRAsnMo** or **MRNAMo**, the vibrational modes at *ca.* 850, *ca.* 625 and *ca.* 520 cm^{-1} have been assigned to ν(O-O), ν_{asym}(Mo-O$_2$) and ν_{sym}(Mo-O$_2$), respectively [26,58-59]. The presence of these bands confirmed the existence of side-on bound peroxido ligand in each of the compounds. Strong absorption at *ca.* 950 cm^{-1} in the spectrum of each of the title compounds was attributable to a terminally bonded Mo=O group [26,58-59].

The strong absorption in the spectrum of the virgin **MR** at 1264 cm^{-1} has been assigned to ν(C-Cl) mode of vibration of –CH$_2$Cl moiety [40,54]. The decrease of band intensity was observed in the spectrum of the functionalized polymers **MRNA** on anchoring of nicotinic acid and in **MRAsn** the band was found absent on anchoring of the amino acid, suggesting replacement of the Cl from the –CH$_2$Cl group of the **MR** by the ligands [40,54].

The IR spectrum of **MRAsn**, apart from showing the characteristic absorptions at *ca.* 3050, 2900, 1025 and 695 cm^{-1} due to $\nu_{aromatic}$(CH), $\nu_{aliphatic}$(CH), $\delta_{aromatic\ in-plane}$(CH) and $\delta_{aromatic\ out-of-plane}$(CH), displayed new bands typical of **Asn** ligand giving clear indication of functionalization of polymeric matrix with the amino acid [26-27,40,54,56,60]. The most prominent band observed at 1629 cm^{-1} in IR spectrum of **MRAsn** has been ascribed to ν(C=O) (amide I) [60-62]. The band due to δ(NH$_3^+$) observed at ca. 1680 cm^{-1} in the spectrum of free asparagine was absent in the spectrum of polymer bound **MRAsn**, indicating the participation of the group in bond formation with the polymer [60]. In addition, the appearance of new band at 1089 cm^{-1} for ν(C–N) indicated the formation of carbon-nitrogen bond by replacing the chloride group of the host resin [26-27,40,54]. The bands due to ν_{asym}(COO) and ν_{sym}(COO) modes of **Asn** occurred at 1600 and 1422 cm^{-1}, respectively in **MRAsn** spectrum [60-62]. After metal incorporation, ν_{asym}(COO) band was observed at a higher frequency of 1696 cm^{-1} whereas, the ν_{sym}(COO) band was shifted to a lower value (1406 cm^{-1}) indicating complexation of the metal through the -COO group [26-27,56,63]. The resulting $\Delta\nu$

[ν_{asym}(COO) - ν_{sym}(COO)] is 290 cm^{-1} for **MRAsnMo** which confirms unidentate coordination of the complex [26-27,56,61]. The unaltered position of the amide bands suggests that the amide group in not involved in coordination with the metal center. The band at 1747 cm^{-1} showed the presence of free -COOH group in the compound (**5.1**). In the low frequency region of the spectrum, appearance of a new band at 575 cm^{-1} indicated the M-N bond formation in the complex [64-65].

In case of the spectrum of niacin grafted **MRNA**, additional bands appeared attributable to ν_{asym}(COO), ν_{sym}(COO) and ν(CN) respectively, apart from the typical absorptions due to **MR** (**Fig. 5.7**, **Table 5.4)**, showing complexation of the ligand to the resin [34-35,66-72]. The band at 1707 and 1417 cm^{-1} for the ν_{asym}(COO) and ν_{sym}(COO) groups of pure ligand remain almost unaltered in **MRNA**. In contrast, the CN vibrational frequency of the ligand at 1087 cm^{-1} was shifted to a positive value of 1110 cm^{-1}, thus providing evidence of anchoring of the ligand to the polymer through the pyridine ring nitrogen atom [35]. Upon anchoring of **pMo** groups to **MRNA**, the spectrum showed a distinct shift of the ν_{asym}(COO) to higher frequency and that of ν_{sym}(COO) group to a lower value, relative to the free pendant ligand values (**Table 5.4)**. The corresponding $\Delta \nu$[ν_{asym}(COO) - ν_{sym}(COO)] was 323 cm^{-1}, which strongly suggests unidentate coordination of the –COO group to the metal [34,35,56,70-73].

The broad absorption bands around 3500-3400 cm^{-1} in the spectra of the title compounds reveal the presence of lattice water. Since the ν(NH) band appear in the same frequency region, therefore, it is not possible to distinguished the two bands with certainty.

The IR results have been corroborated further by the complementary Raman spectral analysis (**Fig. 5.8** - **Fig. 5.9**) which exhibited the well resolved bands corresponding to ν(Mo=O), ν(O-O), ν_{asym}(Mo-O$_2$), ν_{sym}(Mo-O$_2$) vibrations at 954, 846, 622, 523 cm^{-1} for **MRAsnMo (5.1)** and 956, 853, 625, 525 cm^{-1} for **MRNAMo (5.2)** respectively [58-59,74]. Raman spectra of the complexes **5.1** and **5.2** also displayed weak intensity bands for ν_{asym}(COO) and ν_{sym}(COO) modes of vibrations at 1682, 1379 cm^{-1} and 1691, 1369 cm^{-1} respectively. The benzene skeletal vibrations appeared at ca. 1600 and 1000 cm^{-1} as intense peaks in each of the spectra [55,75-76].

Table 5.4 Infrared and Raman spectral data (in cm^{-1}) for polymer support, ligand-anchored Merrifield resin and polymer immobilized peroxido molybdates[a]

Compound		$\nu_{as}(COO)$	$\nu_s(COO)$	$\nu(C-Cl)$	$\nu(Mo=O)$	$\nu(O-O)$	$\nu_{as}(M-O_2)$	$\nu_s(M-O_2)$	Mo-N
MR	IR	--	--	1267(m)	--	--	--	--	--
	R	--	--	1265(m)	--	--	--	--	--
MRAsn	IR	1600(s)	1423(s)	--	--	--	--	--	--
	R	1620(w)	1453(w)	--	--	--	--	--	--
MRAsnMo	IR	1696(s)	1406(s)	--	954(s)	846(s)	523(s)	622(s)	575(s)
	R	1682(vw)	1379(w)	--	943(s)	851(s)	535(m)	638(m)	572(m)
MRNA	IR	1704(m)	1422(s)	1274(w)	--	--	--	--	--
	R	1707(vw)	1441(w)	1273(vw)	--	--	--	--	--
MRNAMo	IR	1698(m)	1375(m, sh)	1276(w)	956(s)	853(s)	525(s)	625(s)	--
	R	1691(w)	1369(w)	1273(vw)	948(s)	857(s)	538(w)	623(m)	--

[a]s, strong; m, medium; w, weak; vw, very weak; sh, shoulder
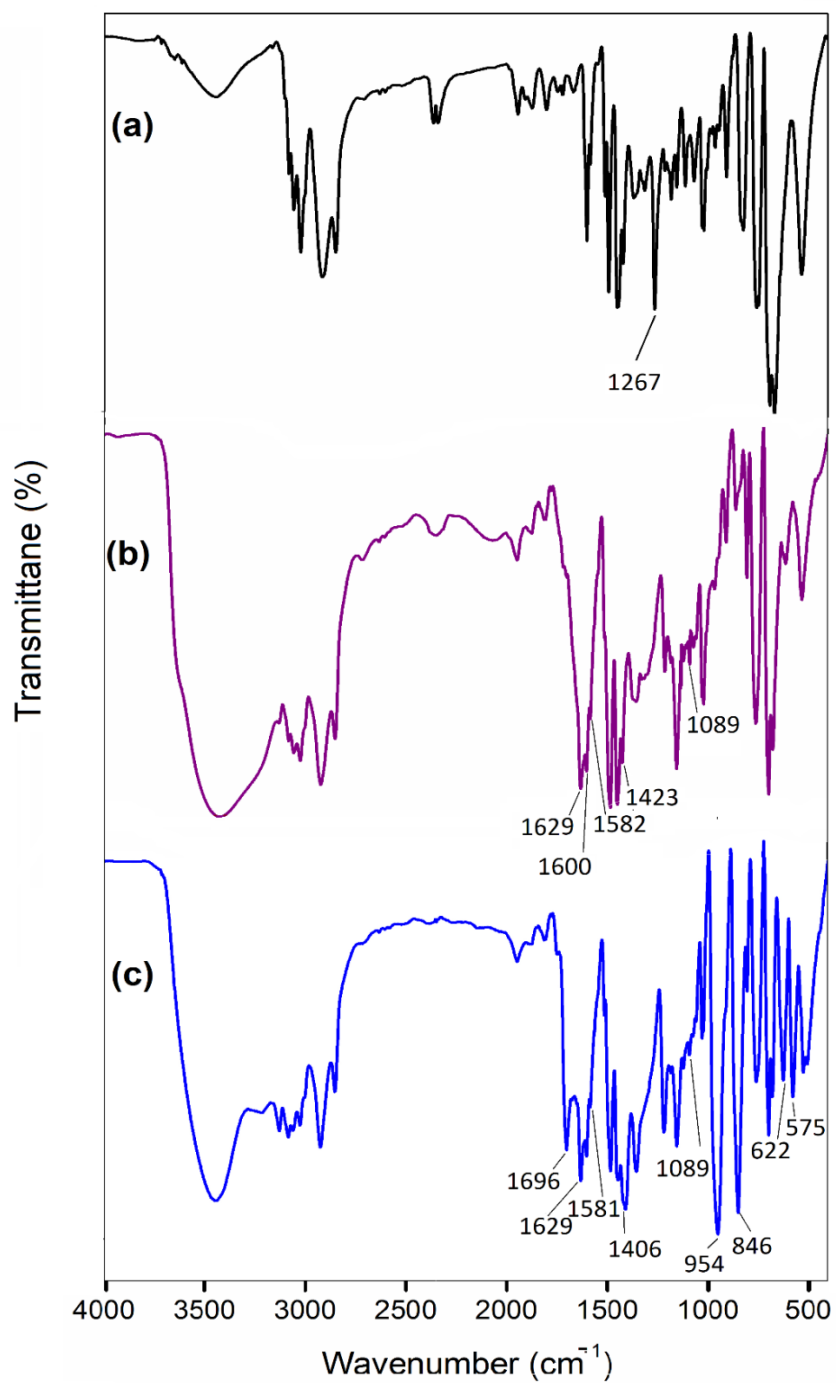
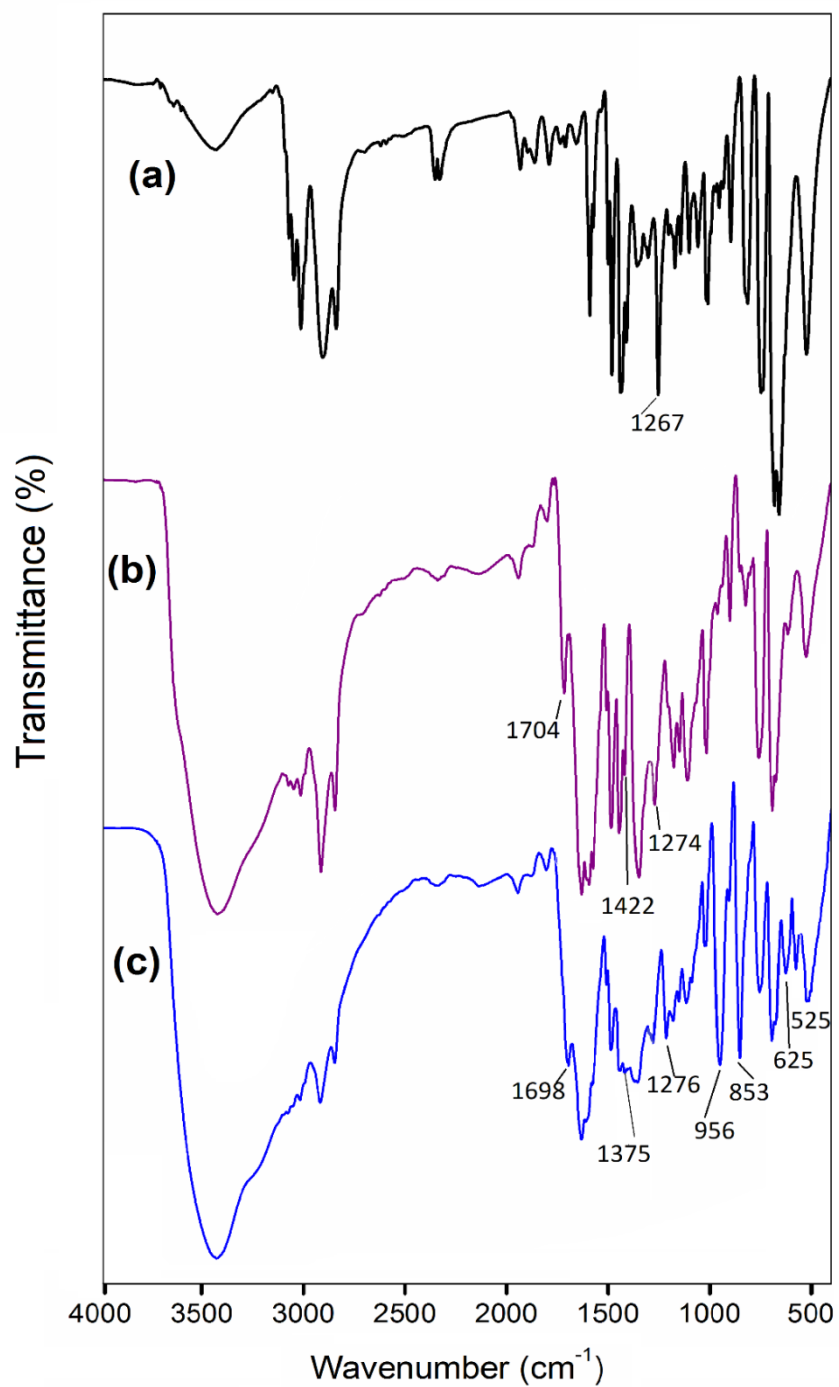**Fig. 5.6** IR spectra of (a) **MR**, (b) **MRAsn** and (c) **MRAsnMo.**

Fig. 5.7 IR spectra of (a) **MR**, (b) **MRNA** and (c) **MRNAMo**.
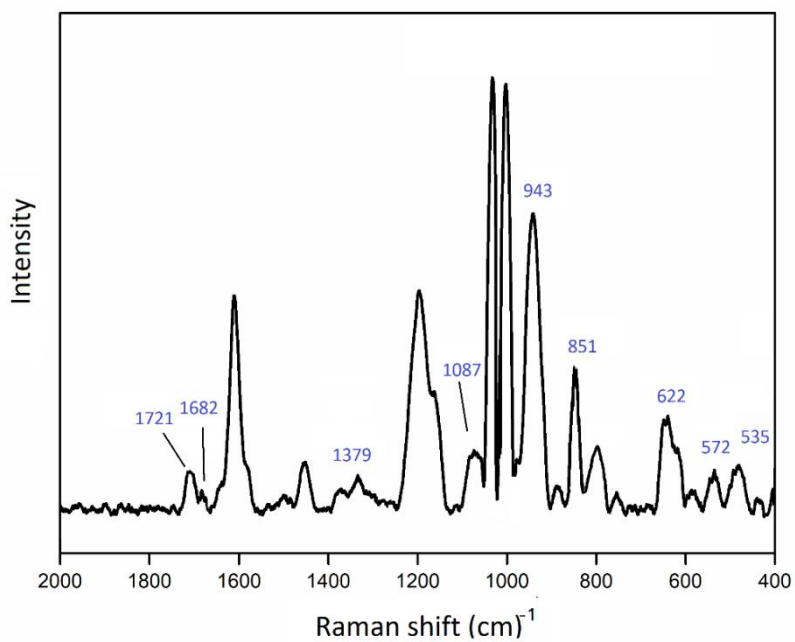
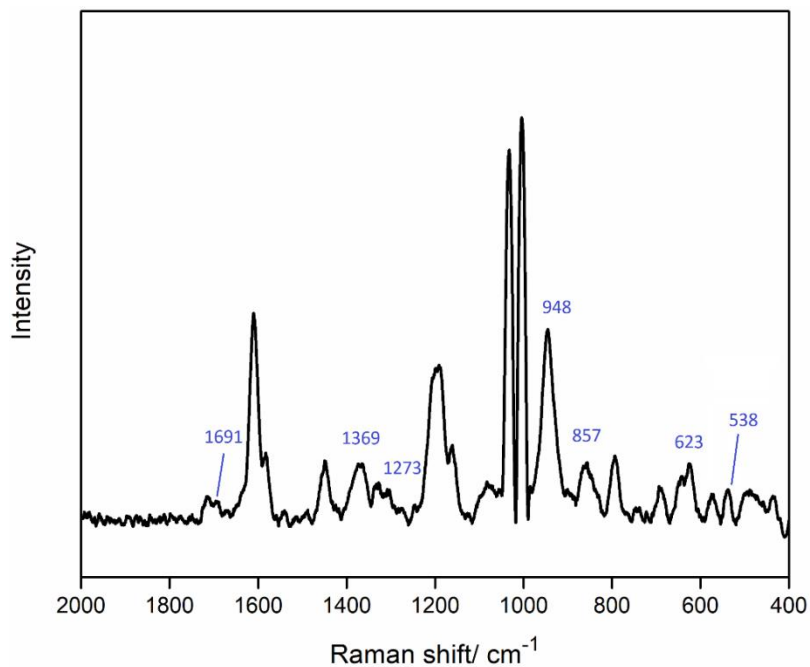**Fig. 5.8** Raman spectrum of **MRAsnMo**.

Fig. 5.9 Raman spectrum of **MRNAMo**.

5.3.2.6 Diffuse reflectance UV–visible analysis

The diffuse reflectance UV–visible spectra of both the compounds **5.1** and 5.**2** exhibited two well-resolved peaks in the region 260-380 nm (**Fig. 5.10** and **Fig. 5.11**). The weaker intensity absorption at *ca.* 360 nm is characteristic of peroxido to metal (LMCT) transition of a monoperoxidomolybdate(VI) species [26,34,7778]. The strong peak at *ca.* 260 nm is attributable to π→π* transitions in the polymeric ligand [78].

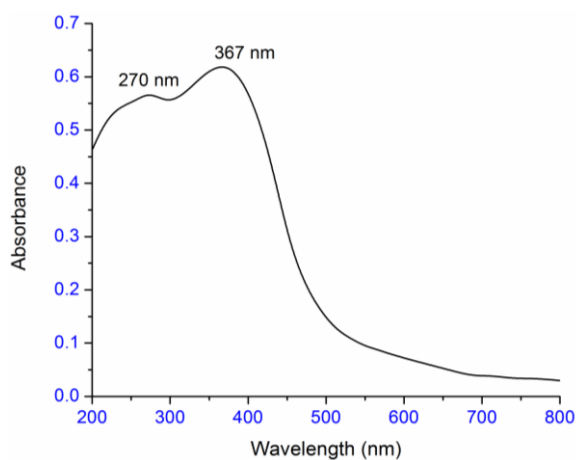**Fig. 5.10** Diffuse reflectance UV–vis spectrum of **MRAsnMo** (**5.1**).
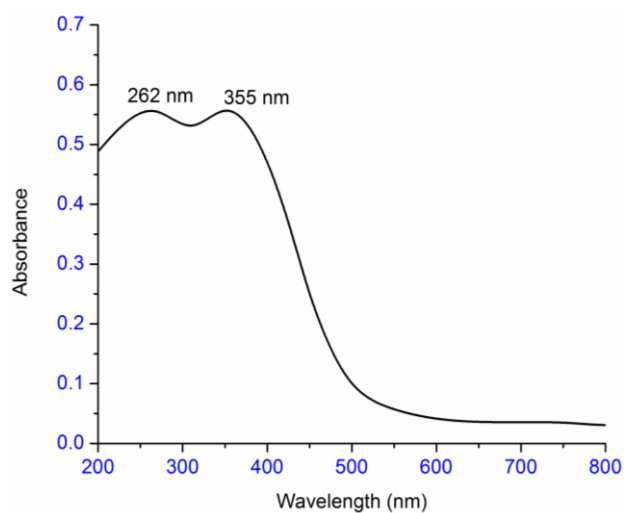

Fig. 5.11 Diffuse reflectance UV–vis spectrum of **MRNAMo** (**5.2**).

5.3.2.7 ^{13}C NMR studies

The solid state ^{13}C NMR spectra of the synthesized complexes are shown in **Fig. 5.12** and **Fig. 5.13**. The corresponding chemical shift data obtained for the compounds in each step of synthesis are presented in **Table 5.5** along with peak assignments, made on the basis of available literature [26-27,66,73,79-85]. The spectra of the pristine polymer and the resins **MRAsn** or **MRNA** displayed characteristic resonances corresponding to quaternary and protonated aromatic as well as aliphatic methine carbons [80]. In addition to these resonances, in the spectra of **MRAsnMo** and **MRNAMo** new peaks appear due to carboxylate carbon at 181 (**MRAsn**) and 165 ppm (**MRNA**), providing evidence for the presence of L-asparagine and niacin in the functionalized polymers [27,66]. Also a closely spaced peak at 179.8 ppm was observed in the spectrum of **MRAsn**, which corresponds to the free amide carbon. Complete removal of Cl from -CH$_2$Cl group by the amino acid in **MRAsn** was evident from the absence of signal at *ca.* 46 ppm. Along with this the appearance of new NMR signal at *ca.* 64 ppm that ascribes to amine bounded carbon of L-asparagine, confirms the presence of C-N bonding in **MRAsn** [26-27,82-83]. On the other hand, the resin **MRNA** exhibited signal at *ca.* 46 ppm along with a new one at *ca.* 64 ppm. While the former is due to the presence of -CH$_2$Cl group, the later peak indicates the bonding of methylene carbon of the polymer to the nitrogen of the pyridine ring of the ligand [26-27,84-85]. Signals of the complexes, that are not detected in the solid state ^{13}C NMR are believed to have been merged with the broad signals for the pure polymer that is present in the major amount.

The NMR spectra of both the catalysts displayed a new peak at considerably lower field of 214.8 ppm (**MRAsnMo**) (**5.1**) and 206.0 ppm (**MRNAMo**) (**5.2**), respectively which are attributable to the metal coordinated carboxylate C atom. Moreover, the significant downfield shift, $\Delta\delta$ ($\delta_{complex} - \delta_{free\ carboxylate}$) $\approx$ 33.1 ppm in case of **MRAsnMo** and *ca.* 39.8 ppm in **MRNAMo** relative to the free carboxylate of the ligand suggest strong metal ligand interaction in the complexes [26-27,73]. The solid state ^{13}C NMR spectral studies thus provided further evidence in support of the functionalization of the resins and formation of the complexes, **MRAsnMo** (**5.1**) and **MRNAMo** (**5.2**).
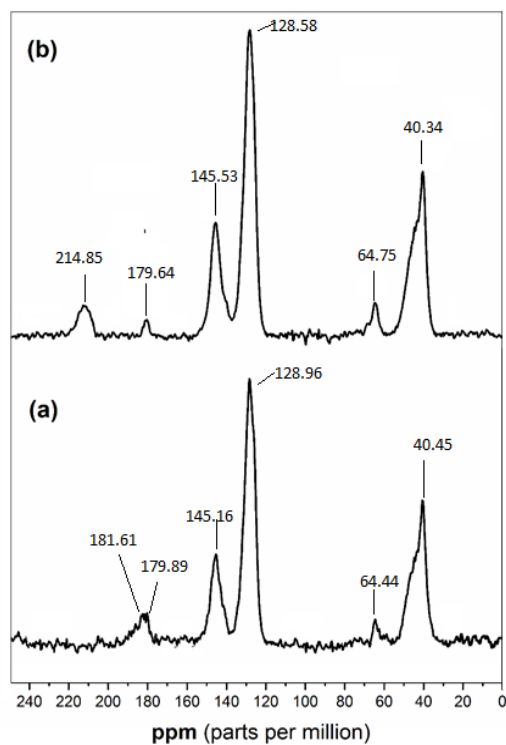
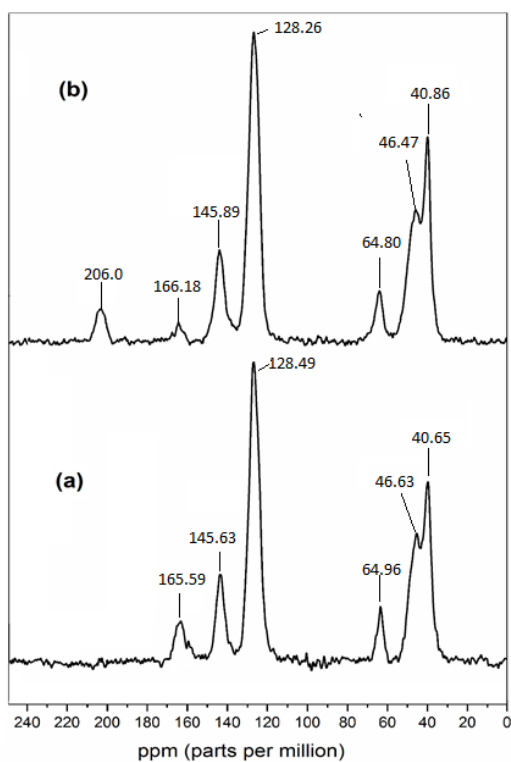**Fig. 5.12** Solid state ^{13}C NMR spectra of (a) **MRAsn** and (b) **MRAsnMo.**

Fig. 5.13 Solid state ^{13}C NMR spectra of (a) **MRNA** and (b) **MRNAMo.**

Table 5.5 ^{13}C NMR chemical shifts for Merrifield resin, ligand-anchored Merrifield resin and polymer bound peroxidomolybdates

Compound	Chemical shift (ppm)								
	Merrifield resin					Ligand			
	Quaternary Aromatic Carbons	Protonated Aromatic Carbons	Aliphatic Methine Carbons	CH$_2$Cl	-CH$_2$N	C-NH	CONH$_2$	Carboxylate Free	Complexed
MR	145.1	128.3	41.0	46.1	--	--	--	--	--
MRAsn	145.1	128.9	40.4	--	--	64.4	179.8	181.6	--
MRAsnMo	145.5	128.5	40.3	--	--	64.7	179.6	--	214.8
MRNA	145.6	128.4	40.6	46.6	64.9	--	--	165.5	--
MRNAMo	145.8	128.2	40.8	46.4	64.8	--	--	166.1	206.0

5.3.2.8 Thermal analysis

It was observed that the compounds undergo multistage of thermal degradation on heating up to a high temperature of 700 ^{0}C under nitrogen atmosphere. The TG plots of the compounds **5.1** and **5.2** are shown in **Fig. 5.14** –**Fig. 5.15** and the data are presented in **Table 5.6**.

As seen in the table, in case of **MRAsn** and **MRNA**, a weight loss of 12.40 % and 6.8% occurs in the temperature range of 143-244 and 163-230 ^{0}C, respectively. On the basis of available literature data on degradation patterns for asparagine and nicotinic acid, we assign this weight loss to the release of ligand amino acid and nicotinic acid from the resins [71,86-88]. Both the functionalized resins show initial weight loss between room temperature and *ca.* 100 ^{0}C due to the liberation of water of crystallization.

After the initial dehydration, the first pronounced weight loss was observed as 4.6% for **MRAsnMo** (**5.1**) in the temperature range of 105-145 ^{0}C. For **MRNAMo** (**5.2**), 2.27% was found at 108-138 ^{0}C. This degradation can be attributed to the complete loss of coordinated peroxido group from the complexes. The IR spectral analysis of the decomposition product isolated at this stage confirms the absence of peroxide. The complexes **5.1** and 5.**2** show 10.0 % and 6.2 % weight losses in the temperature range of 146-297 ^{0}C and 175-264 ^{0}C respectively, which has been ascribed to the loss of the pendent ligands from the resins.

The final step of degradation in the temperature range of 300 to 700 ^{0}C was observed in each of the polymeric compounds with a maximum weight loss (44.0% in complex **5.1** and 59.3% in complex **5.2**). The pure polymer **MR** shows degradation starting from 284 ^{0}C upto 700 ^{0}C and this indicates that the final weight loss was due to the decomposition of the base polymer [89]. The black residue from the **pMo** compounds, after total loss of the components was revealed to be a hydrated oxidomolybdenum species. This was identified from the IR spectra which displayed the characteristic v(Mo=O) and v(OH) absorptions and was devoid of bands due to peroxido and the polymeric ligands of the original catalyst.

Table 5.6 Thermogravimetric data for **MRAsn**, **MRNA**, **MRAsnMo** and **MRNAMo**

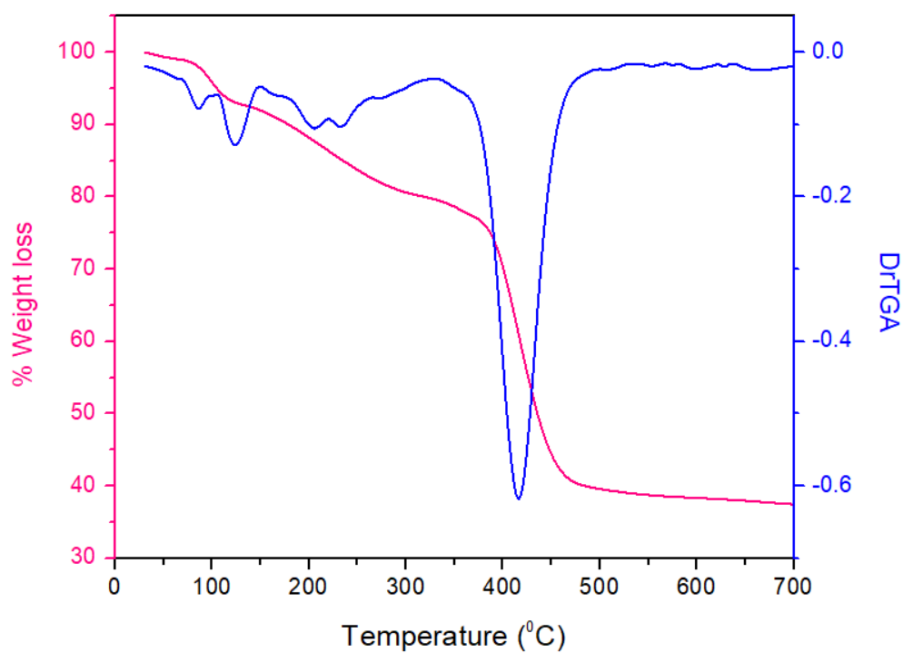| Compound	Temperature range (^{0}C)	Observed weight loss (%)	Final residue (%)
MRAsn	31-98	4.4	12.2
	143-244	12.4	
	248-700	71.0	
MRAsnMo	68-99	3.4	37.8
	105-145	4.6	
	146-297	10.0	
	301-700	44.0	
MRNA	40-83	1.5	10.3
	163-230	6.8	
	231-700	82.3	
MRNAMo	70-99	2.0	30.1
	108-138	2.2	
	175-264	6.2	
	265-700	59.3	

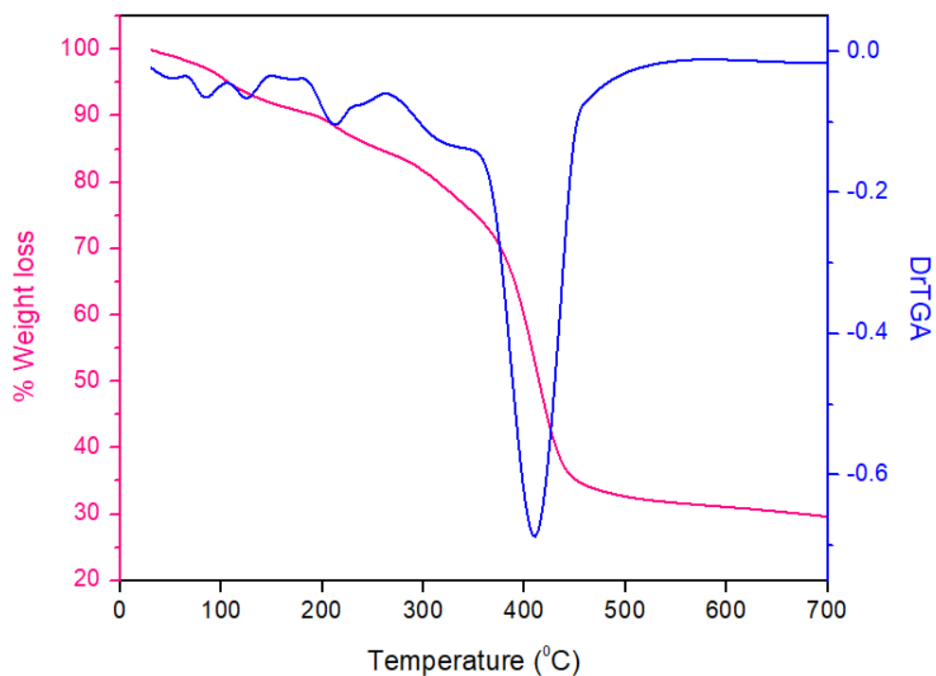**Fig. 5.14** TG-DTG plot of **MRAsnMo**.

Fig. 5.15 TG-DTG plot of **MRNAMo**.

On the basis of the above experimental evidences, structures of the complexes **MRAsnMo (5.1)** and **MRNAMo (5.2)** have been proposed as shown in **Fig. 5.16** where the ligand is coordinated to the polymer (**MR**) *via* the nitrogen atom. The dioxidomonoperoxidomolybdenum(VI) moiety is anchored to the carboxylate group of the pendant ligands in an unidentate fashion, thus completing six fold coordination around each molybdenum centre.
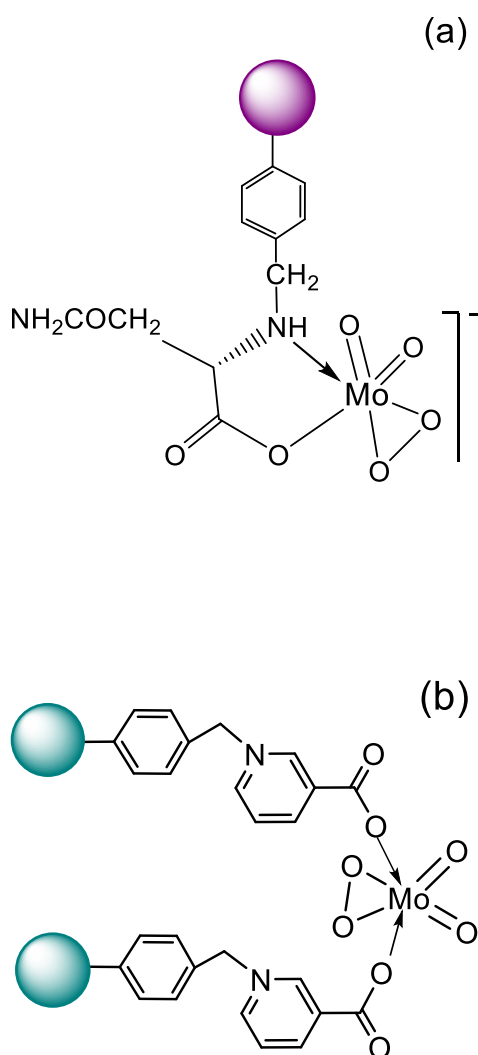

Fig. 5.16 Proposed structure of (a) **MRAsnMo** and (b) **MRNAMo.** "⬤"represents polymer chain.

5.4 Catalytic activity of the synthesized complexes MRAsnMo (5.1) and MRNAMo (5.2) in organic oxidations

5.4.1 Alkene epoxidation

The catalytic activity of the immobilized **pMo** catalysts in epoxidation of olefins was investigated using styrene as the model substrate and **MRAsnMo** as representative catalyst. In order to standardize the reaction conditions for maximum substrate conversion, the influence of various factors such as solvent, the catalyst/substrates molar ratio, the reaction temperature and time etc. was examined.

5.4.1.1 Effect of solvent

To study the solvent effect, we have performed epoxidation reaction in water and various other relatively safer organic solvents, as well as under solvent-free condition. For comparison, all the reactions were conducted under identical reaction condition using 1 equivalent of 30% H_2O_2 as oxidant, 1:1000 catalyst(Mo):substrate molar ratio at 60 ^{0}C. It is evident from the findings summarized in **Table 5.7** and shown in **Fig. 5.17,**
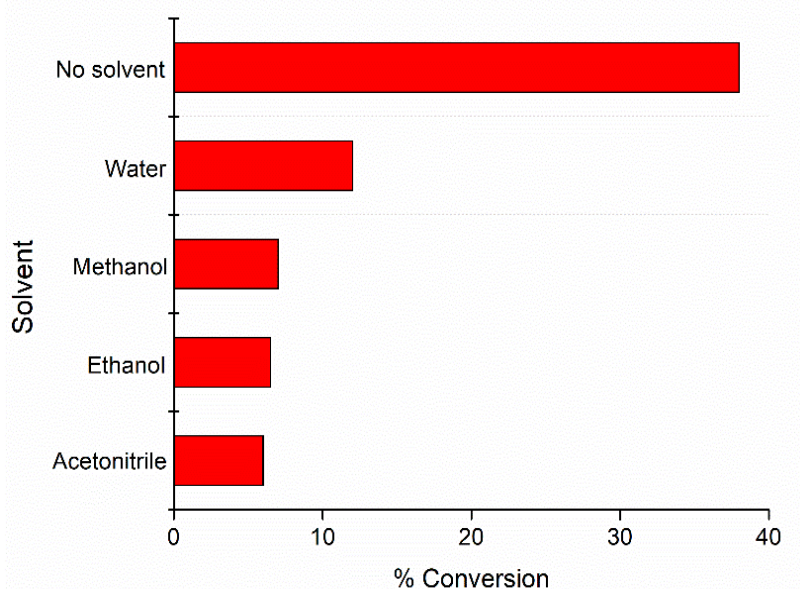

Fig. 5.17 % styrene conversion vs. solvent for catalyst **MRAsnMo**. Reaction conditions: Styrene (5 mmol), catalyst (0.005 mmol of Mo, 2.8 mg), 30% H_2O_2 (5 mmol, 0.56 mL), 60 ^{0}C, solvent (5 mL), 1 h.

Table 5.7 Effect of solvent on styrene oxidation with 30% H_2O_2 catalyzed by **MRAsnMo (5.1)**[a]

Entry	Solvent	Solvent Volume (mL)	Conversion (%)	Selectivity (%)	TON[b]	TOF[c] (h^{-1})
1	MeOH	5	≥7	100	70	70
2	EtOH	5	≥6.5	100	65	65
3	CH$_3$CN	5	≥6	100	60	60
4	H$_2$O	5	≥12	100	120	120
5	H$_2$O	3	≥15	100	150	150
6	H$_2$O	1	≥17	≥ 99	170	170
7	--	--	≥38	≥ 99	380	380

[a]Reaction conditions: Styrene (5 mmol), catalyst (0.005 mmol of Mo, 2.8 mg), 30% H_2O_2 (5 mmol, 0.56 mL), 60 ^{0}C, solvent (5 mL), 1 h. [b]TON (turn over number)= mmol of product per mmol of catalyst. [c]TOF (turn over frequency) = mmol of product per mmol of catalyst per hour.

that under these conditions, the best results in terms of higher styrene conversion with nearly 100% epoxide selectivity was attained under solvent free condition with a TOF of 380 h^{-1} within just 1 h of reaction time.

It is notable that despite the low conversion recorded in presence of organic solvents, the reaction proceeded to yield epoxide as sole product in each case. It has also been observed that with a decrease in the solvent volume a slight increase in conversion occurred (**Table 5.7**, entries 5 and 6). Thus the observed negative impact of solvent on the outcome of styrene epoxidation reaction as compared to the higher efficiency of the solvent-free procedure, may possibly be linked to the restricted mobility experienced by the reactants in absence of solvent in the reaction mixture. Based on these results, we continued further studies on styrene epoxidation under solvent free condition.

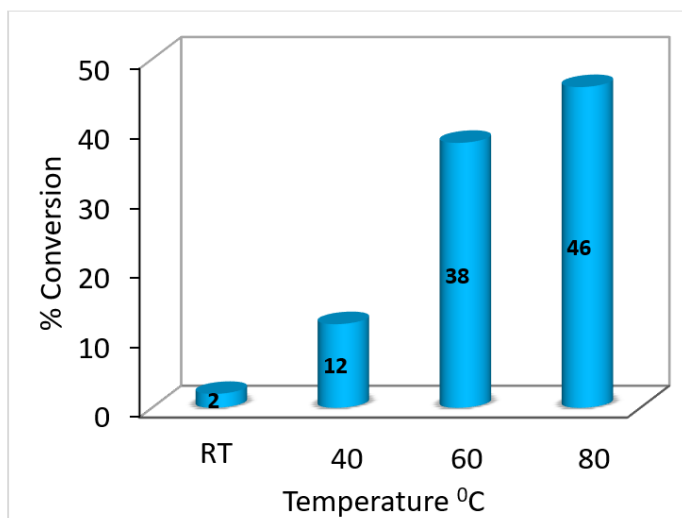## 5.4.1.2 Effect of temperature

Fig. 5.18 % styrene conversion vs. temperature for catalyst **MRAsnMo**. Reaction conditions: Styrene (5 mmol), catalyst amount (0.005 mmol of Mo, 2.8 mg), 30% H_2O_2 (5 mmol, 0.56 mL), 1 h.

The effect of temperature on the conversion of styrene is shown in **Fig. 5.18**. Starting from room temperature, the reaction was performed independently under four different reaction temperatures, viz, 40, 60, 80 ^{0}C, keeping other reaction parameters constant. The results revealed that with the rise in temperature the conversion increased gradually to provide a good conversion with highest TOF value of ~ 460 h^{-1} (**Table 5.8**, entry 4) at 80 ^{0}C, within 1 h without any significant effect on epoxide selectivity. These results prompted us to evaluate further styrene epoxidation reaction at 80 ^{0}C of temperature.

Table 5.8 Effect of temperature on styrene oxidation with 30% H_2O_2 catalyzed by **MRAsnMo**(**5.1**)[a]

Entry	Temperature (^{0}C)	Conversion (%)	Selectivity (%)	TON[b]	TOF[c] (h^{-1})
1	RT	≥2	100	20	20
2	40	≥12	100	120	120
3	60	≥38	≥ 99	380	380
4	80	≥46	≥ 99	460	460

[a]Reaction conditions: Styrene (5 mmol), catalyst (0.005 mmol of Mo, 2.8 mg), 30% H_2O_2 (5 mmol, 0.56 mL), 1 h. [b]TON(turn over number)= mmol of product per mmol of catalyst. [c]TOF (turn over frequency) = mmol of product per mmol of catalyst per hour.

5.4.1.3 Effect of H₂O₂ concentration

The influence of oxidant amount on the reaction rate was studied using five different equivalents of 30% H_2O_2 with respect to substrate. The results illustrated in **Fig. 5.19** show a consistent negative trend in % conversion of styrene with increase in styrene : oxidant ratio from 1:1 to 1:5 under identical reaction condition and running the reaction for 1 h. Thus, the relatively high conversion was observed at 1:1:: styrene: H_2O_2 molar ratio (**Table 5.9**, entry 1), whereas in a reaction performed maintaing 1:5::styrene:H_2O_2 molar ratio a significant decrease in conversion occurred (**Table 5.9**, entry 5). Thus, it was gratifying to note that a stoichiometric amount of H_2O_2 with respect to styrene was optimal to achieve reasonable good conversion along with ≥99% selectivity of the target product. The factor possibly responsible for the observed trend appears to be the dilution of the reacting species in the reaction mixture, which occur due to addition of increasing volumes of oxidant. As revealed by earlier reports [27,90-91], such observation is not unusual in case of H_2O_2 induced metal-catalyzed organic oxidations.
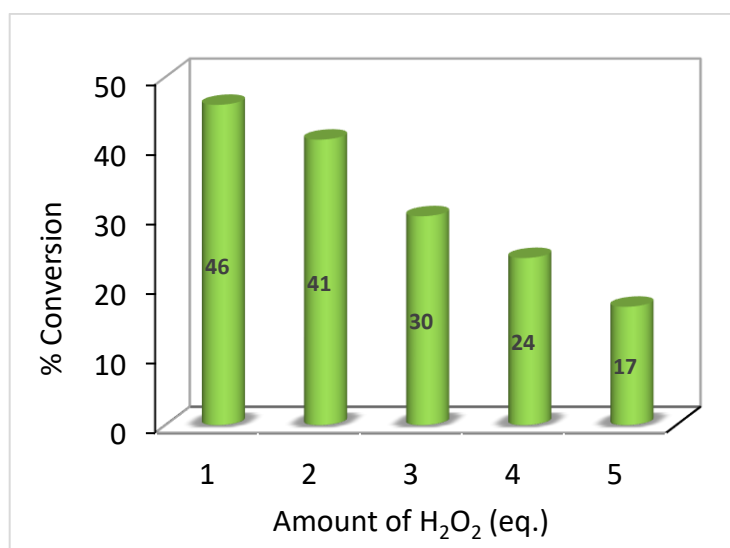

Fig. 5.19 % styrene conversion vs. amount of H_2O_2 (eq.) for catalyst **MRAsnMo**. Reaction conditions: Styrene (5 mmol), catalyst (0.005 mmol of Mo, 2.8 mg), 80 ^{0}C, 1 h.

Table 5.9 Effect of H_2O_2 concentration on the styrene oxidation with 30% H_2O_2 catalyzed by **MRAsnMo** (**5.1**)[a]

Entry	Sub: H_2O_2	Conversion (%)	Selectivity (%)	TON[b]	TOF[c] (h^{-1})
1	1:1	≥ 46	≥ 99	460	460
2	1:2	≥ 41	≥ 99	410	410
3	1:3	≥ 30	100	300	300
4	1:4	≥ 24	100	240	240
5	1:5	≥ 17	100	170	170

[a]Reaction conditions: Styrene (5 mmol), catalyst (0.005 mmol of Mo, 2.8 mg), 80 ^{0}C, 1h. [b]TON (turn over number)= mmol of product per mmol of catalyst. [c]TOF (turn over frequency) = mmol of product per mmol of catalyst per hour.

5.4.1.4 Effect of catalyst amount

The influence of catalyst:substrate molar ratio on rate of styrene epoxidation is shown in **Table 5.10**. It is evident that increase in the amount of catalyst keeping the other parameters constant, led to considerable enhancement of styrene conversion without any significant loss of selectivity (**Fig. 5.20**). It is remarkable that, even at a considerably lower catalyst concentration (**Table 5.10**, entry 4), the reaction proceeded to afford a high TON or TOF value of 480 h^{-1} with 100% epoxide selectivity. A comparable TOF value was also obtained with 1:1000 of catalyst:substrate molar ratio with an improved conversion. Therefore, this value was chosen as optimal for further epoxidation reactions (**Table 5.10**, entry 3). Although the conversion could be increased further by increasing the catalyst amount, the resulting TOF and TON values showed a steady decrease (**Table 5.10**, entry 1).

A blank experiment carried out in absence of the catalyst under standard condition afforded only 5% conversion within the stipulated reaction time (**Table 5.10**, entry 5), signifying the role of the catalyst in facilitating the oxidation reaction. Furthermore, a reaction conducted by using Na_2MoO_4 in lieu of the catalyst, **MRAsnMo** under identical reaction condition yielded poor conversion (**Table 5.10**, entry 6), testifying to the superior activity of the immobilized **pMo** catalysts *vis-à-vis* the free **pMo** species generated in solution.
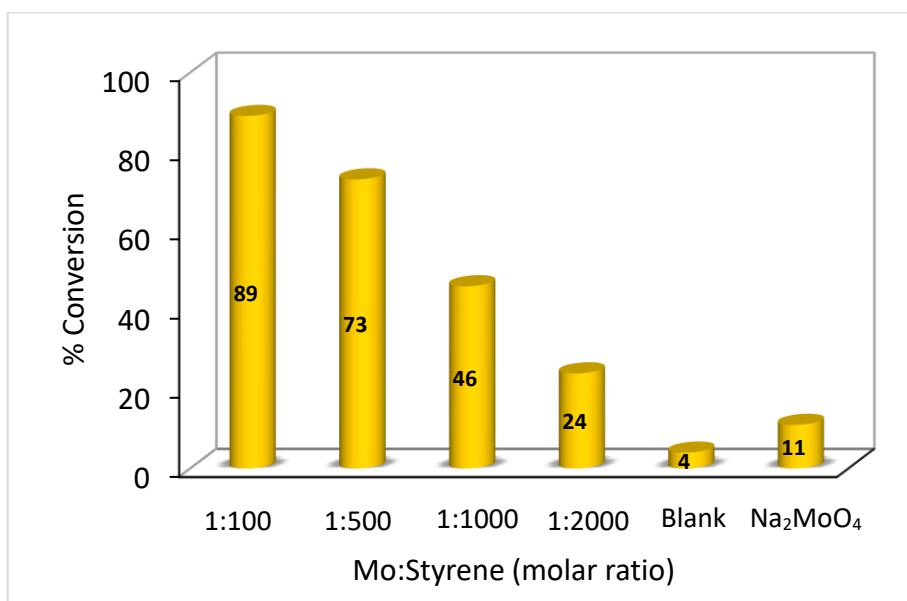
Fig. 5.20 % styrene conversion vs. catalyst amount (mmol of Mo). Reaction conditions: Styrene (5 mmol), 30% H_2O_2 (5 mmol, 0.56 mL), 80 ^{0}C, 1 h.

Table 5.10 Effect of catalyst amount on styrene oxidation with 30% H_2O_2 catalyzed by **MRAsnMo** (**5.1**)[a]

Entry	Molar ratio Mo:Styrene	Conversion (%)	Selectivity (%)	TON[b]	TOF[c] (h^{-1})
1	1:100	≥89	≥ 98	89	89
2	1:500	≥73	≥ 99	365	365
3	1:1000	≥46	≥ 99	460	460
4	1:2000	≥24	100	480	480
5	--	≥4[d]	100	--	--
6	1:1000	≥11[e]	≥ 97	110	110

[a]Reaction conditions: Styrene (5 mmol), 30% H_2O_2 (5 mmol, 0.56 mL), 80 ^{0}C, 1h. [b]TON (turn over number)= mmol of product per mmol of catalyst. [c]TOF (turn over frequency) = mmol of product per mmol of catalyst per hour. [d]Blank experiment without catalyst. [e]Using Na_2MoO_4 (1.02 mg, 0.005 mmol) as catalyst.

5.4.1.5 Effect of reaction time

The % conversion profile of styrene as a function of time is depicted in **Table 5.11** and **Fig. 5.21.** The trend obtained after monitoring the reaction over a span of 6 h, showed that after the rapid conversion occurring within initial 30 minutes of starting the reaction, there was a steady rise in TON till complete conversion was attained at 6 h. (**Table 5.11**, entries 1 and 2). Thus, it is noteworthy that the conversion of 31% occurring within initial 30 min of starting the reaction resulted in the best TOF value (620 h^{-1}) obtained for the oxidation process. Importantly, the results also demonstrate that the catalyst retained its activity as well as epoxide selectivity profile even after 6 h of reaction time notwithstanding the reasonably high temperature at which the reaction was conducted.

Table 5.11 Effect of reaction time on styrene oxidation with 30% H$_2$O$_2$ catalyzed by **MRAsnMo (5.1)**[a]

Entry	Time (h)	Conversion (%)	Selectivity (%)	TON[b]	TOF[c] (h^{-1})
1	0.5	≥31	100	310	620
2	1	≥46	≥99	460	460
3	2	≥59	≥99	590	295
4	3	≥74	≥99	740	247
5	4	≥81	≥99	810	202
6	5	≥93	≥99	930	186
7	6	≥100	≥99	1000	167

[a]Reaction conditions: Styrene (5 mmol), catalyst (0.005 mmol of Mo, 2.8 mg), 30% H$_2$O$_2$ (5 mmol, 0.56 mL), 80 ^{0}C. [b]TON (turn over number)= mmol of product per mmol of catalyst. [c]TOF (turn over frequency) = mmol of product per mmol of catalyst per hour.
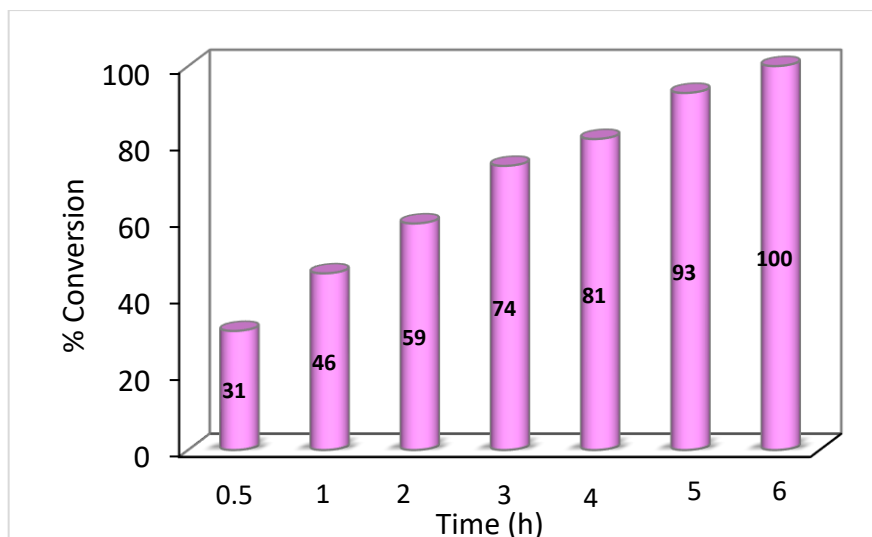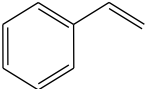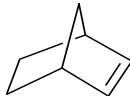
Fig. 5.21 % styrene conversion vs. reaction time for catalyst **MRAsnMo**. Reaction conditions: Styrene (5 mmol), catalyst (0.005 mmol of Mo, 2.8 mg), 30% H_2O_2 (5 mmol, 0.56 mL), 80 ^{0}C.

Subsequent to establishing the standard condition for styrene oxidation with catalyst **5.1**, the scope of the methodology in oxidation of a number of structurally different alkene substrates were investigated under same condition using both the catalysts **MRAsnMo** and **MRNAMo**. As evident from the data presented in **Table 5.12**, entries 1-4, catalyst **5.1** displayed slightly superior efficiency in epoxidation relative to catalyst **5.2**. Significantly, cyclooctene and norbornene were completely oxidized to provide the targeted epoxide with nearly 100% selectivity within *ca.* 2 h, although in case of cyclohexene the epoxide selectivity was moderate. Surprisingly, no report appears to exist on norbornene epoxidation catalyzed by molybdenum-based catalyst under solvent free condition.

.

Table 5.12 selective oxidation of alkene to epoxides with 30% H_2O_2, catalyzed by **MRAsnMo** and **MRNAMo**

Entry	Substrate	MRAsnMo							MRNAMo					
		Time (h)	Conversion (%)	Selectivity epoxide	Selectivity others	TON[b]	TOF[c]		Time (h)	Conversion (%)	Selectivity epoxide	Selectivity others	TON[b]	TOF[c]
1		6	100	≥99	1[d]	1000	167		6	≥82	≥99	1[d]	820	137
		6	≥97[e]	≥99	1[d]	970	162		6	≥80[e]	≥98	2[d]	800	133
		6	100[f]	≥99	1[d]	1000	167		6	≥84[f]	≥99	1[d]	840	140
2		2	100	≥76	24[g]	760	380		2.5	100	≥73	27[g]	730	292
3		2	100	100	--	1000	500		2.2	100	100	--	1000	456
4		1.5	100	≥98	2[h]	1000	667		2	100	≥97	3[h]	970	485

[a]Reactions were carried out with 5 mmol substrate, 5 mmol of 30% H_2O_2 without solvent at 80 ^{0}C. Catalyst (0.005 mmol of Mo), [b]TON (turn over number)= mmol of product per mmol of catalyst. [c]TOF (turn over frequency) = mmol of product per mmol of catalyst per hour. [d]Benzaldehyde. [e]% Conversion for 6th reaction cycle. [f]Scale up reaction. [g]2-cyclohexen-1-ol, 2-cyclohexen-1-one, 2-Hydroxy-1-cyclohexanone, [h]Norbornanone.

5.4.2 Sulfide oxidation

5.4.2.1 Oxidation of sulfides to sulfoxides

Encouraged by the excellent catalytic activity displayed by the supported **pMo** catalysts in alkene epoxidation, we first examined their efficacy in selective oxidation of sulfide to sulfoxides under same optimized condition using methyl phenyl sulfide (MPS) as a model substrate in absence of solvent. Under these conditions however, the reaction product obtained was a mixture of sulfoxide and sulfone and thus was non-selective (**Table 5.13**, entry 1). We have therefore, explored the reaction using **MRAsnMo** as catalyst in presence of variety of solvents and evaluated the effect of various reaction parameters as illustrated in **Table 5.13**. As evident from the data, the reaction conducted in water was observed to be sluggish and non-selective (entry 2). We could finally achieve the best results in terms complete conversion as well as 100% sulfoxide selectivity by conducting the reaction at room temperature in MeOH using 2 equivalents of 30% H_2O_2 and maintaining a catalyst : MPS molar ratio of 1:3000. To our pleasure, the reaction under these conditions was completed within a very short time of 5 min despite the very less amount of catalyst used, leading to a remarkably high TOF of 35,084 h^{-1}. Further increase in the oxidant or catalyst amount however, led to overoxidation of sulfide and formation of sulfone as byproduct, lowering the product selectivity. Therefore, the condition in **Table 5.13**, entry 10 was considered as optimal for further oxidation reactions.

The optimized condition for selective sulfoxidation was further exploited to obtain pure sulfoxide from a series of structurally diverse organic sulfides listed in **Table 5.14**. The maximum TOF for selective product formation was observed for dimethyl sulfide (**Table 5.14**, entry 2). However, high conversion with excellent TOF values were also obtained for dibutyl sulfide, methyl p-tolyl sulfide, allyl phenyl sulfide, dihexyl sulfide, and thioanisol. The trend expected in variation of rates of these oxidations across the substrates studied, has been found to be consistent with the decreasing nucleophilicity of the thioethers examined, as has been mentioned in Chapters 3 and 4. The ability of both the catalysts to chemoselectively oxidize sulfur group of substituted sulfides containing additional oxidation-prone functional groups is also evident from **Table 5.14** (entries 7 and 8).
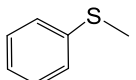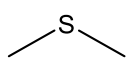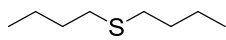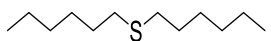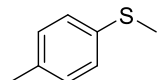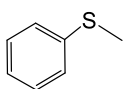
Table 5.13 Optimization of reaction conditions for **MRAsnMo** catalyzed selective oxidation of methyl phenyl sulfide (MPS) by 30% $H_2O_2{}^a$
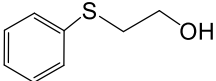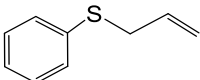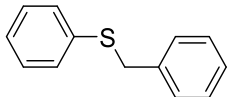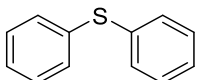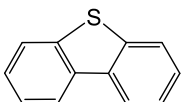
Entry	Molar ratio (Mo:MPS)	H_2O_2 Equiv.	Solvent	Time (min)	Isolated yield (%)	1a:1b	TON[b]	TOF[c] (h^{-1})
1	1:1000	2	--	115	96	74:26	960	502
2	1:1000	2	H_2O	135	97	65:45	970	431
3	1:1000	2	MeOH	5	98	60:40	980	11807
4	1:1000	2	EtOH	10	97	85:15	970	5705
5	1:1000	2	CH_3CN	5	97	80:20	970	11686
6	1:500	2	MeOH	5	98	42:58	490	5903
7	1:1500	2	MeOH	5	97	82:18	1469	17698
8	1:2000	2	MeOH	5	98	92:8	1960	23614
9	1:2500	2	MeOH	5	96	97:3	2400	28915
10	**1:3000**	**2**	**MeOH**	**5**	**99**	**100:0**	**2912**	**35084**
11	1:3000	3	MeOH	5	98	73:27	2882	34722
12[d]	1:3000	2	MeOH	5	11	88:12	323	3891
13[e]	--	2	MeOH	5	5	100:0	--	--

[a]Reactions were carried out in 5 mmol of substrate, 30% H_2O_2 in 5 mL of solvent at room temperature. Catalyst (2.8 mg for 0.005 mmol of Mo). [b]TON(turn over number)=mmol of product per mmol of catalyst. [c]TOF(turn over frequency)= mmol of product per mmol of catalyst per hour. [d]Using Na_2MoO_4 as catalyst (0.34 mg, 0.0017 mmol of Mo). [e]Blank experiment without any catalyst.

Table 5.14: Selective oxidation of sulfides to sulfoxides with 30% H_2O_2 catalyzed by **MRAsnMo** and **MRNAMo** at room temperature[a]

MRAsnMo or **MRNAMo** (Mo: S =1:3000)

30% H_2O_2 (2 equivalents), RT, MeOH

Entry	Substrate	MRAsnMo				MRNAMo			
		Time (min)	Isolated yield (%)	TON[b]	TOF[c] (h^{-1})	Time (min)	Isolated yield (%)	TON[b]	TOF[c] (h^{-1})
1		5	99	2912	35084	8	98	2882	22169
			97[d]	2853	34373		96[d]	2823	21715
2		3	96	2823	56460	5	95	2794	33662
3		5	98	2882	34723	7	96	2823	24128
4		5	95	2794	33662	8	97	2853	21946
5		5	96	2823	34012	8	95	2794	21492
6		7	98	2882	24632	10	98	2882	16952

Continued...
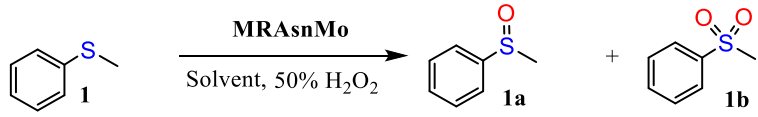
Entry	Substrate								
7	PhS-CH2CH2OH	15	97	2853	11412	20	96	2823	8554
8	PhS-CH2CH=CH2 (allyl phenyl sulfide)	15	96	2823	11292	17	98	2882	10183
9	benzyl phenyl sulfide	18	98	2882	9606	22	97	2853	7710
10	diphenyl sulfide	45	96	2823	3764	60	97	2853	2853
11[e]	dibenzothiophene	10 h	95	475	47.5	10.5	93	465	44.2

[a]All reactions were carried out in 5 mmol substrates, 10 mmol 30% H_2O_2 and catalyst (0.0017 mmol of Mo) in 5 mL methanol at RT, unless otherwise indicated. [b]TON (turnover number) = mmol of product per mmol of catalyst. [c]TOF (turnover frequency) = mmol of product per mmol of catalyst per hour. [d]Yield of 10th reaction cycle. [e]Reaction condition: 5 mmol substrate, 10 mmol 30% H_2O_2 and catalyst (0.01 mmol of Mo) at 65 °C in refluxing methanol.

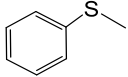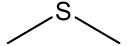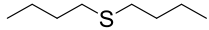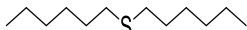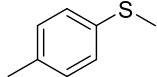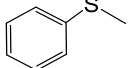### 5.4.2.2 Oxidation of sulfide to sulfone under solvent free condition

The immobilized catalysts could further be successfully applied to obtain sulfone as the exclusive product by using 50% H_2O_2 as oxidant. Most importantly, complete conversion of MPS to pure sulfone could be achieved in presence of organic solvents as well as without solvent. However, the best TOF value for the conversion of sulfide to sulfone was obtained under solvent free condition by conducting the reaction at room temperature maintaining 1:1000::catalyst:substrate molar ratio, using 3 equivalents of oxidant under the conditions mentioned in **Table 5.15** (entry 9). The data presented in **Table 5.16** further demonstrate that the developed oxidation protocol is highly effective for a variety of organic sulfides. The remarkable chemoselectivity of the catalysts toward sulfur group was evident in case of its oxidation to sulfone as well, notwithstanding the presence of excess of 50% H_2O_2 in the reaction mixture.

Table 5.15 Optimization of reaction conditions for the **MRAsnMo** catalyzed selective oxidation of methyl phenyl sulfide (MPS) to sulfone by 50% $H_2O_2^a$
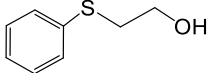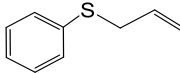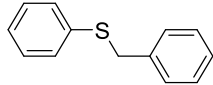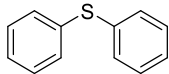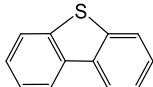

Entry	Molar ratio (Mo:MPS)	H_2O_2 Equiv.	Solvent	Temp. (^0C)	Time (min)	Isolated yield (%)	1a:1b	TON[b]	TOF[c] (h^{-1})
1	1:500	4	H_2O	RT	300	97	12:88	485	97
2	1:500	4	MeOH	RT	180	98	0:100	490	163
3	1:500	4	CH_3CN	RT	175	96	0:100	480	165
4	1:500	4	MeOH	65 ^0C	65	97	0:100	485	447
5	1:500	4	CH_3CN	78 ^0C	50	98	0:100	490	588
6	1:500	4	--	RT	25	97	0:100	485	1164
7	1:500	3	--	RT	15	98	0:100	490	1960
8	1:100	3	--	RT	5	98	0:100	98	1176
9	**1:1000**	**3**	**--**	**RT**	**30**	**99**	**0:100**	**990**	**1980**
10	1:2000	3	--	RT	75	98	0:100	1960	1568
11	1:1000	4	--	RT	90	98	0:100	980	653
12	1:1000	2	--	RT	45	99	0:100	990	1320

[a]All the reactions were carried out with 5 mmol of substrate in 5 mL of solvent. [b]TON (turnover number) = mmol of product per mmol of catalyst. [c]TOF (turnover frequency) = mmol of product per mmol of catalyst per hour.

Table 5.16 Selective oxidation of sulfides to sulfones with 50% H_2O_2 catalyzed by **MRAsnMo** and **MRNAMo** at room temperature[a]

Entry	Substrate	MRAsnMo				MRNAMo			
		Time (min)	Isolated yield (%)	TON[b]	TOF[c] (h^{-1})	Time (min)	Isolated yield (%)	TON[b]	TOF[c] (h^{-1})
1		30	99	990	1980	40	98	980	1462
			96[d]	960	1920		96[d]	960	1432
2		17	97	970	3427	25	96	960	2307
3		25	98	980	2355	35	97	970	1663
4		30	97	970	1940	40	96	960	1432
5		35	98	980	1689	40	97	970	1447
6		45	98	980	1306	60	96	960	960

#	Structure								
7		95	98	980	620	115	96	960	501
8		55	97	970	1057	70	96	960	820
9[e]		135	98	980	436	150	96	960	384
10		150	97	970	388	165	96	960	349
11[f]		12 h	94	470	39	12h	92	460	38.3

[a]All reactions were carried out in 5 mmol substrates, 15 mmol 50% H_2O_2 and catalyst (0.005 mmol of Mo) under solvent free condition at RT, unless otherwise indicated. [b]TON (turnover number) = mmol of product per mmol of catalyst. [c]TOF (turnover frequency) = mmol of product per mmol of catalyst per hour. [d]Yield of 6th reaction cycle. [e]Reaction condition: 5 mmol substrate, 15 mmol 50% H_2O_2 and catalyst (0.005 mmol of Mo) in 5 mL acetonitrile at RT. [f]Reaction condition: 5 mmol substrate, 15 mmol 50% H_2O_2 and catalyst (0.01 mmol of Mo) at 78°C in refluxing acetonitrile.

5.4.3 Recyclability of the catalysts

Reusability of the supported catalysts was examined independently in alkene epoxidation and sulfide oxidation using styrene or thioanisole as substrate under respective optimized reaction condition. After recovering the catalyst by filtration followed by washing with acetone and drying under vacuum, it was recharged in subsequent reaction run. The recyclability of the synthesized catalysts was evaluated for six consecutive cycles of reaction in case of solvent-free styrene epoxidation as well as oxidation of sulfide to sulfone. On the other hand, for selective sulfoxidation, recyclability was examined up to ten cycles. From the data presented in (**Table 5.12**, entry 1), (**Table 5.14**, entry 1) and (**Table 5.16**, entry 1) that in each type of oxidation, activity and selectivity of the catalysts remain undiminished even after repeated cycles of oxidation (**Fig. 5.22- Fig. 5.24**).

We have characterized each recovered catalyst by FTIR, Raman, ICP-OES and EDX spectral analysis. Comparable IR, Raman and EDX spectral patterns of original and recovered catalysts confirmed that the catalysts remain stable during the catalytic process. Also, ICP analysis indicated the absence of Mo in the filtrate after isolating the solid catalyst, thereby negating the possibility of catalyst leaching. Moreover, no further
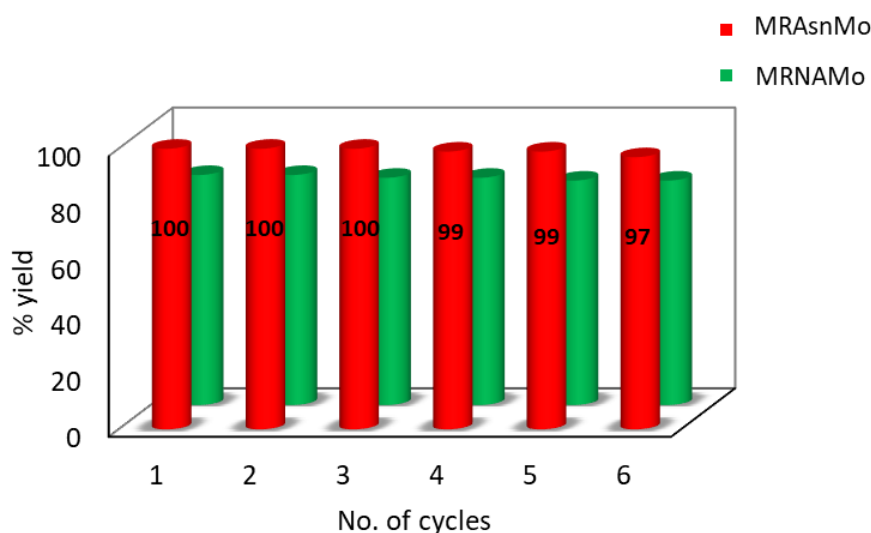
Fig. 5.22 Recyclability of catalysts **MRAsnMo** and **MRNAMo** for selective oxidation of styrene.
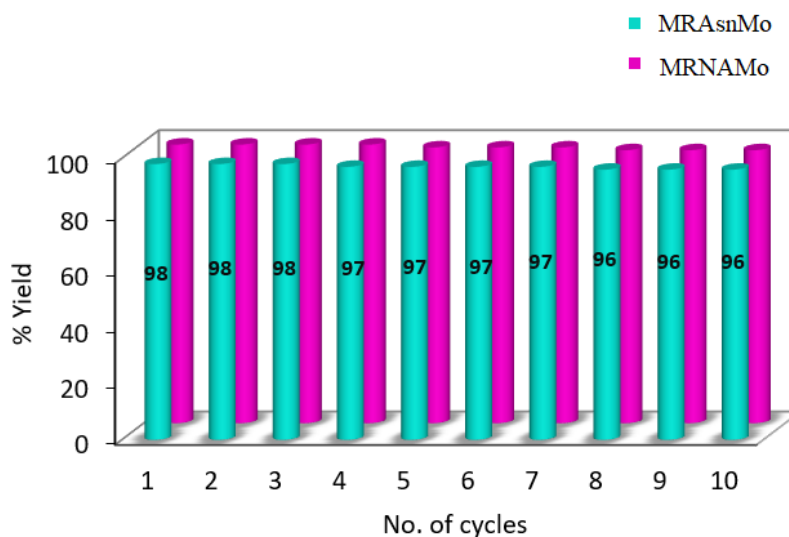
Fig. 5.23 Recyclability of catalyst **MRAsnMo** and **MRNAMo** for the selective oxidation of MPS to sulfoxide in MeOH.

conversion was noted after separation of the solid catalyst from reaction mixture and allowing the reaction to continue for another 1 h under optimized conditions. These results demonstrate the heterogeneous nature of the catalytic process.
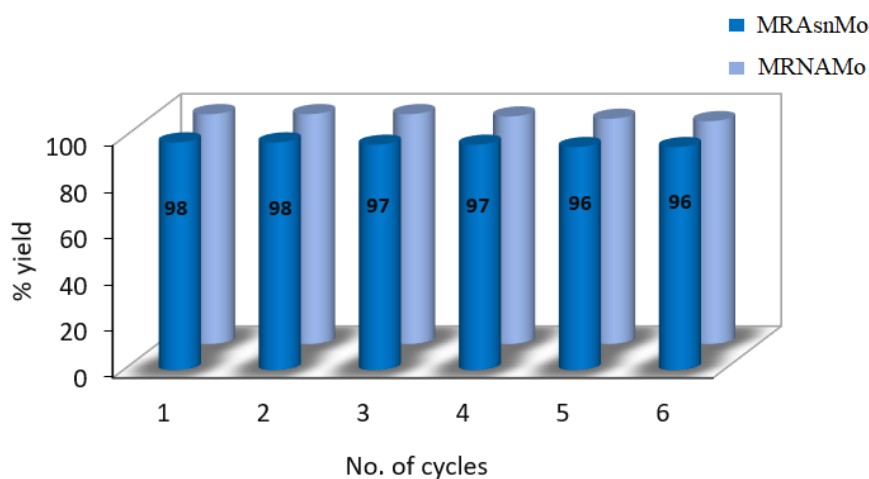

Fig. 5.24 Recyclability of catalysts **MRAsnMo** and **MRNAMo** for the selective oxidation of sulfide to sulfone under solvent-free condition.

5.4.4 Proposed catalytic cycle

On the basis of experimental evidences, supported by results of theoretical investigation it has already been established by work from several laboratories that, epoxidation reactions catalyzed by d^0 transition metal peroxido systems of metals such as V(V), Mo(VI), W(VI) usually follow a common reaction pathway which involve the direct electrophilic transfer of the oxygen atom of the peroxido group to the alkene through a spiro-like transition state in a concerted step [92-96].

Based on the findings of the present study and aforementioned available literature, we have proposed a catalytic cycle for the selective styrene epoxidation mediated by the supported oxidomonoperoxidomolybdenum catalysts **MRAsnMo** and **MRNAMo**. As shown in **Fig. 5.25**, the first step involves the formation of active diperoxidomolybdate species **II** from the inactive monoperoxidomolybdate species **I** in the presence of excess H_2O_2, as mentioned in chapter 4 (section 4.2.3.6). In the next step the diperoxidomolybdate species **II** would transfer its electrophilic oxygen to the alkene (reaction a) through an intermediate **III** followed by formation of a spirocyclic structure as suggested by Sharpless *et al.* [92-94]. In the final step of the catalytic cycle, the product will dissociate from the intermediate **IV** (reaction b) to yield the respective epoxide and subsequently generate the original catalyst **I**.

The catalytic cycle envisaged for selective oxidation of sulfides to their corresponding sulfoxides or sulfones is outlined in **Fig. 5.26**, using **MRAsnMo** as representative catalyst. As mentioned in Chapter 5, in presence of excess H_2O_2, the diperoxidomolybdate species **II** (reaction a) is likely to be generated from the monoperoxidomolybdate species **I** which would transfer its electrophilic oxygen to the substrate **V** to yield the corresponding sulfoxide **VI**. The sulfoxidation reaction is accompanied by simultaneous regeneration of the original catalyst **I**. In a separate cycle of reaction, diperoxidomolybdate species **II** may further oxidize sulfoxide leading to sulfone formation (reaction c). Thus, formation of sulfone appears to be a two step process [26,98-102].
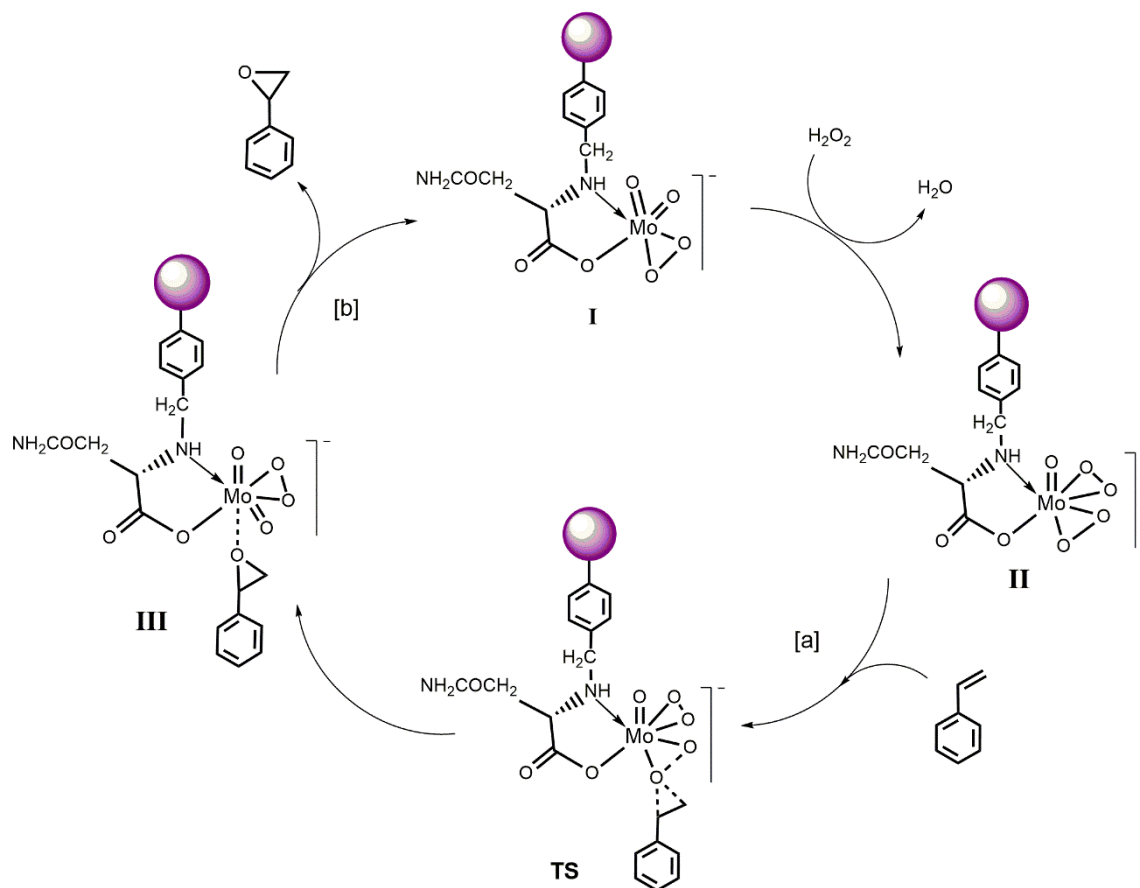
Fig 5.25 Proposed catalytic cycle for alkene epoxidation with heterogeneous catalyst shown with **MRAsnMo (5.1)** as representative in presence of H_2O_2.

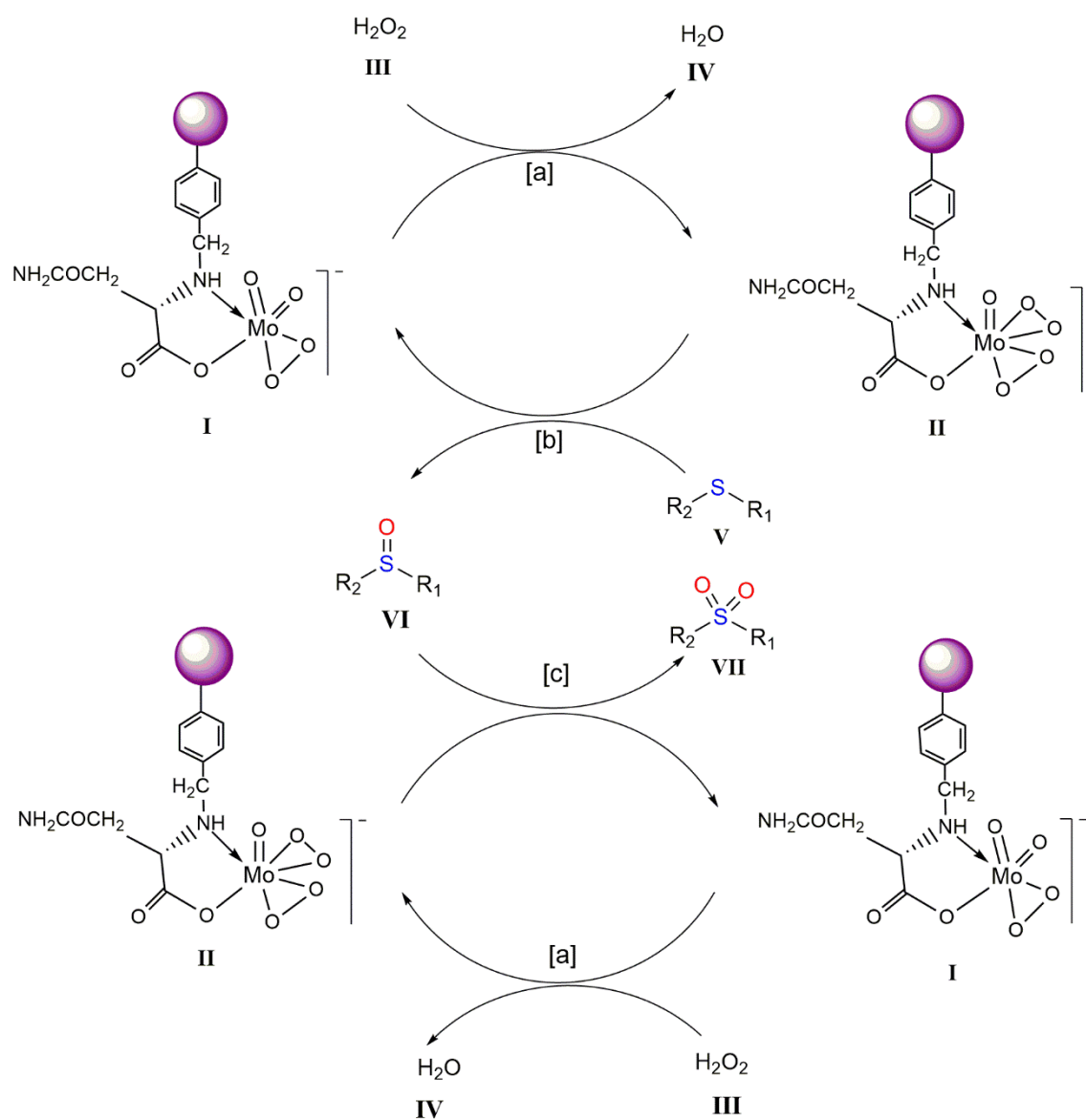**Fig. 5.26** Proposed catalytic cycle for sulfide oxidation with heterogeneous catalyst shown with **MRAsnMo (5.1)** as representative in presence of H_2O_2.

5.5 Conclusion

To conclude, we have introduced a pair of new heterogeneous catalysts prepared by immobilizing peroxidomolybdenum species on asparagine and niacin grafted Merrifield resin which demonstrated great potential for the environmentally benign epoxidation of variety of alkenes with H_2O_2 under mild and solvent free condition. It is noteworthy that complete conversion of unfunctionalized alkenes has been achieved with nearly 100% epoxide selectivity employing just stoichiometric amount of 30% H_2O_2 in absence of organic solvent. Moreover, a remarkably high turn over number of *ca.* 1000 was obtained in each case of epoxidations. These findings appear to be indeed impressive taking into account the mild reactions conditions employed and considering the fact that, in most of the reported solvent free alkene epoxidation processes catalyzed by heterogeneous Mo-based systems used TBHP as oxidant and required much higher temperature [22,47,103-105].

The versatility of these catalysts is further evident from their ability to facilitate the chemoselective oxidation of a broad range of structurally diverse thioethers to the desired sulfoxides in impressive yield and TOF in methanol at ambient temperature. In fact, a TOF of 56,460 h^{-1} obtained using catalyst **5.1**, appears to be one of the highest TOF values obtained in selective sulfoxidation using Mo based catalysts reported so far.

The catalysts afforded easy recovery with reusability for multiple reaction cycles with undiminished activity and selectivity in all cases. Most importantly, the methodologies are environmentally clean as the oxidations have been carried out in absence of halogenated solvent, co-solvent, co-catalysts or any other acid or base additives. Ease of preparation of the catalysts involving a non-toxic transition metal and commercially available starting materials, simplicity in work-up procedure, are the other synthetically valuable attributes of the catalytic systems making them potentially attractive for practical applications.

References

1. Roberts, S. M. and Whittall, J. *Regio- and Stereo-Controlled Oxidations and Reductions*. Wiley-Interscience, New York, 2007.

2. Cavani, F. and Teles, J. H. Sustainability in catalytic oxidation: an alternative approach or a structural evolution? *ChemSusChem: Chemistry and Sustainability, Energy and Materials*, 2(6):508-534, 2009.

3. Bauer, K., Garbe, D., and Surburg, H. *Common fragrance and flavor materials: preparation, properties and uses*. John Wiley & Sons, Newyork, 2008.

4. Caron, S., Dugger, R. W., Ruggeri, S. G., Ragan, J. A., and Ripin, D. H. B. Large-scale oxidations in the pharmaceutical industry. *Chemical Reviews*, 106(7):2943-2989, 2006.

5. Song, Y., Xin, F., Zhang, L., and Wang, Y. Oxidation of Cyclohexene in the Presence of Transition-Metal-Substituted Phosphotungstates and Hydrogen Peroxide: Catalysis and Reaction Pathways. *ChemCatChem*, 9(21):4139-4147, 2017.

6. Amini, M., Haghdoost, M. M., and Bagherzadeh, M. Oxido-peroxido molybdenum (VI) complexes in catalytic and stoichiometric oxidations. *Coordination Chemistry Reviews*, 257(7-8):1093-1121, 2013.

7. Conte, V. and Bortolini, O. Transition Metal Peroxides. Synthesis and Role in Oxidation Reactions. In Marek, I., editor, *PATAI'S Chemistry of Functional Groups*, ISBN:9780470682531. John Wiley & Sons, New York, 2009.

8. Sherrington, D. C. Polymer-supported metal complex alkene epoxidation catalysts. *Catalysis Today*, 57(1-2):87-104, 2000.

9. Corma, A. From microporous to mesoporous molecular sieve materials and their use in catalysis. *Chemical Reviews*, 97(6):2373-2420, 1997.

10. Sheldon, R. A. Synthetic and mechanistic aspects of metal-catalyzed epoxidations with hydroperoxides. *Journal of Molecular Catalysis*, 7(1):107-126, 1980.

11. Thomas, J. M., Raja, R., and Lewis, D. W. Single-site heterogeneous catalysts. *Angewandte Chemie International Edition*, 44(40):6456-6482, 2005.

12. Liang, J., Liang, Z., Zou, R., and Zhao, Y. Heterogeneous catalysis in zeolites, mesoporous silica, and metal–organic frameworks. *Advanced Materials*, 29(30):1701139, 2017.

13. Morlanés, N. and Notestein, J. M. Grafted Ta–calixarenes: Tunable, selective catalysts for direct olefin epoxidation with aqueous hydrogen peroxide. *Journal of Catalysis*, 275(2):191-201, 2010.

14. Dusi, M., Mallat, T., and Baiker, A. Epoxidation of functionalized olefins over solid catalysts. *Catalysis Reviews*, 42(1-2):213-278, 2000.

15. Notestein, J. M., Iglesia, E., and Katz, A. Grafted metallocalixarenes as single-site surface organometallic catalysts. *Journal of the American Chemical Society*, 126(50):16478-16486, 2004.

16. Bonino, F., Damin, A., Ricchiardi, G., Ricci, M., Spanò, G., D'Aloisio, R., Zecchina, A., Lamberti, C., Prestipino, C., and Bordiga, S. Ti-peroxo species in the TS-1/H_2O_2/H_2O system. *The Journal of Physical Chemistry B*, 108(11):3573-3583, 2004.

17. Tanaka, K. and Toda, F. Solvent-free organic synthesis. *Chemical Reviews*, 100(3):1025-1074, 2000.

18. Noyori, R., Aoki, M., and Sato, K. Green oxidation with aqueous hydrogen peroxide. *Chemical Communications*, (16):1977-1986, 2003.

19. Jones, C. W. *Applications of Hydrogen Peroxide and Derivatives*. Royal Society of Chemistry, Cambridge, 1999.

20. Lane, B. S. and Burgess, K. Metal-catalyzed epoxidations of alkenes with hydrogen peroxide. *Chemical Reviews*, 103(7):2457-2474, 2003.

21. Shen, Y., Jiang, P., Wai, P. T., Gu, Q., and Zhang, W. Recent Progress in Application of Molybdenum-Based Catalysts for Epoxidation of Alkenes. *Catalysts*, 9(1):31, 2019.

22. Zare, M., Moradi-Shoeili, Z., Esmailpour, P., Akbayrak, S., and Özkar, S. Oxazine containing molybdenum (VI)–oxodiperoxo complex immobilized on SBA-15 as highly active and selective catalyst in the oxidation of alkenes to epoxides under solvent-free conditions. *Microporous and Mesoporous Materials*, 251:173-180, 2017.

23. Herbert, M., Alvarez, E., Cole-Hamilton, D. J., Montilla, F., and Galindo, A. Olefin epoxidation by hydrogen peroxide catalysed by molybdenum complexes in ionic liquids and structural characterisation of the proposed intermediate dioxoperoxomolybdenum species. *Chemical Communications*, 46(32):5933-5935, 2010.

24. Gupta, K. C., Sutar, A. K., and Lin, C. C. Polymer-supported Schiff base complexes in oxidation reactions. *Coordination Chemistry Reviews*, 253(13-14):1926-1946, 2009.

25. Merrifield, R. B. Solid phase peptide synthesis. I. The synthesis of a tetrapeptide. *Journal of the American Chemical Society*, 85(14):2149-2154, 1963.

26. Boruah, J. J., Das, S. P., Ankireddy, S. R., Gogoi, S. R., and Islam, N. S. Merrifield resin supported peroxomolybdenum(VI) compounds: recoverable heterogeneous catalysts for the efficient, selective and mild oxidation of organic sulfides with H_2O_2. *Green Chemistry*, 15(10):2944-2959, 2013.

27. Saikia, G., Ahmed, K., Rajkhowa, C., Sharma, M., Talukdar, H., and Islam, N. S. Polymer immobilized tantalum (v)–amino acid complexes as selective and recyclable heterogeneous catalysts for oxidation of olefins and sulfides with aqueous H_2O_2. *New Journal of Chemistry*, 43(44):17251-17266, 2019.

28. Gergely, A., Nagypal, I., and Farkas, E. Thermodynamic relations of parent and mixed complexes of asparagine and glutamine with copper (II). *Journal of Inorganic and Nuclear Chemistry*, 37(2):551-555, 1975.

29. Lomozik, L., and Wojciechowska, A. Comparative studies of the coordination mode in complexes of copper with asparagine and copper with aspartic acid in solution and solid state. *Polyhedron*, 8(1):1-6, 1989.

30. Dávid, Á., Hartman, É. T., Lihi, N., Sóvágó, I., and Várnagy, K. Complex formation of nickel (ii) and zinc (ii) ions with peptide fragments of rat amylin. *New Journal of Chemistry*, 42(10):8131-8136, 2018.

31. Lim, M. C. Mixed-ligand complexes of palladium (II). Part 2. Diaqua (ethylenediamine) palladium (II) complexes of L-asparagine and L-glutamine. *Journal of the Chemical Society, Dalton Transactions*, (14):1398-1400, 1977.

32. Sóvágó, I., Kállay, C., and Várnagy, K. Peptides as complexing agents: Factors influencing the structure and thermodynamic stability of peptide complexes. *Coordination Chemistry Reviews*, 256(19-20):2225-2233, 2012.

33. Verma, S. K. and Bhojak, N. A review on coordination behaviour and bioac-tivity of metal complexes of nicotinic acid and its derivatives. *World Journal of Pharmaceutical Sciences*, 6:490-514, 2017.

34. Djordjevic, C., Puryear, B. C., Vuletic, N., Abelt, C. J., and Sheffield, S. J. Preparation, spectroscopic properties, and characterization of novel peroxo

complexes of vanadium (V) and molybdenum (VI) with nicotinic acid and nicotinic acid N-oxide. *Inorganic Chemistry*, 27(17):2926-2932, 1988.

35. Nazir, M. and Naqvi, I. I. Synthesis, spectral and electrochemical studies of complex of uranium(IV) with pyridine-3-carboxylic acid. *American Journal of Analytical Chemistry*, 4(3):134-140, 2013.

36. Shara, M., Kincaid, A. E., Limpach, A. L., Sandstrom, R., Barrett, L., Norton, N., Bramble, J.D., Yasmin, T., Tran, J., Chatterjee, A., and Bagchi, M. Long-term safety evaluation of a novel oxygen-coordinated niacin-bound chromium(III) complex. *Journal of Inorganic Biochemistry*, 101(7):1059-1069, 2007.

37. Shara, M., Yasmin, T., Kincaid, A. E., Limpach, A. L., Bartz, J., Brenneman, K. A., Chatterjee, A., Bagchi, M., Stohs, S.J., and Bagchi, D. Safety and toxicological evaluation of a novel niacin-bound chromium(III) complex. *Journal of Inorganic Biochemistry*, 99(11):2161-2183, 2005.

38. Jensen, N. L. *U.S. Patent No. 4,923,855*. Washington, DC: U.S. Patent and Trademark Office, 1990.

39. Szymańska, A., Nitek, W., Mucha, D., Karcz, R., Pamin, K., Połtowicz, J., and Łasocha, W. Structural studies and physico-chemical properties of new oxodiperoxomolybdenum complexes with nicotinic acid. *Polyhedron*, 60:39-46, 2013.

40. Valodkar, V. B., Tembe, G. L., Ravindranathan, M., Ram, R. N., and Rama, H. S. A study of synthesis, characterization and catalytic hydrogenation by polymer anchored Pd(II)-amino acid complexes. *Journal of Molecular Catalysis A: Chemical*, 202(1-2):47-64, 2003.

41. Fu Yuanbo, Chen Zhang, Song Wenchao, Yang Wei, Zhou Shijun, Li Yu, Liang Mingrui, Gao Cheng, *Patent No. CN103435541A*. Chinese Patent, 2013.

42. McNamara, C. A., Dixon, M. J., and Bradley, M. Recoverable catalysts and reagents using recyclable polystyrene-based supports. *Chemical Reviews*, 102(10):3275-3300, 2002.

43. Gil, S., Gonzalez, R., Mestres, R., Sanz, V., and Zapater, A. Alkene epoxidations catalysed by Mo (VI) supported on Merrifield's polymer. *Reactive and Functional Polymers*, 42(1), 65-72, 1999.

44. Li, S., Wang, K., Chang, K. C. A., Zong, M., Wang, J., Cao, Y.G., Bai, Y.H., Wei, T.M., and Zhang, Z. Preparation and evaluation of nano-hydroxyapatite/poly

(styrene-divinylbenzene) porous microsphere for aspirin carrier. *Science China Chemistry*, 55(6):1134-1139, 2012.

45. Kim, J. W., Kim, K. J., Park, S. Y., Jeong, K. U., and Lee, M. H. Preparation and characterizations of C60/polystyrene composite particle containing pristine C60 clusters. *Bulletin of the Korean Chemical Society*, 33(9):2966-2970, 2012.

46. Biradar, A. V., Sathe, B. R., Umbarkar, S. B. and Dongare, M. K. Selective cis-dihydroxylation of olefins using recyclable homogeneous molybdenum acetylide catalyst. *Journal of Molecular Catalysis A: Chemical*, 285(1-2):111-119, 2008.

47. Babaei, B., Bezaatpour, A., Amiri, M., Szunerits, S. and Boukherroub, R. Magnetically Reusable $MnFe_2O_4$ Nanoparticles Modified with Oxo-Peroxo Mo (VI) Schiff-Base Complexes: A High Efficiency Catalyst for Olefin Epoxidation under Solvent-Free Conditions. *ChemistrySelect*, 3(10):2877-2881, 2018.

48. Bezaatpour, A., Askarizadeh, E., Akbarpour, S., Amiria, M. and Babaei, B. Green oxidation of sulfides in solvent-free condition by reusable novel Mo (VI) complex anchored on magnetite as a high-efficiency nanocatalyst with eco-friendly aqueous H_2O_2. *Molecular Catalysis*, 436:199-209, 2017.

49. Brunauer, S., Emmett, P. H., and Teller, E. Adsorption of gases in multimolecular layers. *Journal of the American Chemical Society*, 60(2):309-319, 1938.

50. Barrett, E. P., Joyner, L. G., and Halenda, P. P. The determination of pore volume and area distributions in porous substances. I. Computations from nitrogen isotherms. *Journal of the American Chemical society*, 73(1):373-380, 1951.

51. Sing, K. S., Everett, D. H., Haul, R. A. W., Moscou, L., Pierotti, R. A., Rouquerol, J., and Siemieniewska, T. Reporting Physisorption Data for Gas/Solid Systems with Special Reference to the Determination of Surface Area and Porosity. *Pure and Applied Chemistry*, 57(4):603-619, 1985.

52. Gregg, S. J. and Sing, K. S. W. Adsorption, Surface Area and Porosity. Academic Press, London, 1982.

53. Park, S. J., Seo, D. I., and Nah, C. Effect of acidic surface treatment of red mud on mechanical interfacial properties of epoxy/red mud nanocomposites. *Journal of Colloid and Interface Science*, 251(1):225-229, 2002.

54. Valodkar, V. B., Tembe, G. L., Ravindranathan, M., and Rama, H. S. Catalytic epoxidation of olefins by polymer-anchored amino acid ruthenium complexes. *Reactive and Functional Polymers*, 56(1):1-15, 2003.

55. Altava, B., Burguete, M. I., Garcıa-Verdugo, E., Luis, S. V., and Vicent, M. J. The use of NIR-FT-Raman spectroscopy for the characterization of polymer-supported reagents and catalysts. *Tetrahedron*, 57(41):8675-8683, 2001.

56. Nakamoto, K. *Infrared and Raman Spectra of Inorganic and Co-ordination Compounds, Part B*. Wiley and Sons, New York, 1997.

57. Korbély, B., Kiss, J. T., Hernádi, K., and Pálinkó, I. Amino acids and their Cu complexes covalently grafted onto a polystyrene resin–A vibrational spectroscopic study. *Journal of Molecular Structure*, 834:345-348, 2007.

58. Campbell, N. J., Dengel, A. C., and Griffith, W. P. Studies on transition metal peroxo complexes—X. The nature of peroxovanadates in aqueous solution. *Polyhedron*, 8(11):1379-1386,1989.

59. Lever, A. B. P. and Gray, H. B. Electronic spectra of metal-dioxygen complexes. *Accounts of Chemical Research*, 11(9):348-355, 1978.

60. Casado, J., Lopez Navarrete, J. T., and Ramirez, F. J. Infrared and Raman spectra of l-asparagine and l-asparagine-d5 in the solid state. *Journal of Raman Spectroscopy*, 26(11):1003-1008, 1995.

61. Masilamani, S., Ilayabarathi, P., Maadeswaran, P., Chandrasekaran, J., and Tamilarasan, K. Synthesis, growth and characterization of a novel semiorganic nonlinear optical single crystal: l-Asparagine cadmium chloride monohydrate. *Optik*, 123(14):1304-1306, 2012.

62. Venyaminov, S. Y. and Kalnin, N. N. Quantitative IR spectrophotometry of peptide compounds in water (H_2O) solutions. I. Spectral parameters of amino acid residue absorption bands. *Biopolymers: Original Research on Biomolecules*, 30(13-14):1243-1257, 1990.

63. Deacon, G. B. and Phillips, R. J. Relationships between the carbon-oxygen stretching frequencies of carboxylato complexes and the type of carboxylate coordination. *Coordination Chemistry Reviews*, 33(3):227-250, 1980.

64. Şakıyan, İ. Synthesis and characterization of four new manganese (III) complexes and amino acid (L-aspartic acid, L-asparagine, L-glutamic acid, L-glutamine) Schiff bases. *Transition Metal Chemistry*, 32(1):131-135, 2007.

65. Al-Noor, T. H., Mahdi, R. T., and Ismail, A. H. SYNTHESIS, Spectroscopic Characterization and Evaluation (Antibacterial & (GOT, G pT) Enzyme) Activity of Mixed Ligand Complexes of M (II) with Amino Acid (L-Asparagine) and Schiff

Bases Derived from (Sulfamethoxazo Drug with 2, 4Dimethoxybenzaldehyde). *SYNTHESIS*, 31, 2015.

66. Broadhurst, C. L., Schmidt, W. F., Reeves III, J. B., Polansky, M. M., Gautschi, K., and Anderson, R. A. Characterization and structure by NMR and FTIR spectroscopy, and molecular modeling of chromium (III) picolinate and nicotinate complexes utilized for nutritional supplementation. *Journal of Inorganic Biochemistry*, 66(2):119-130, 1997.

67. Lewandowski, W., Barańska, H., and Mościbroda, P. Vibrational study of nicotinic acid complexes with different central ions. *Journal of Raman Spectroscopy*, 24(12):819-824, 1993.

68. Kumar, M. and Yadav, R. A. Experimental IR and Raman spectra and quantum chemical studies of molecular structures, conformers and vibrational characteristics of nicotinic acid and its N-oxide. *Spectrochimica Acta Part A: Molecular and Biomolecular Spectroscopy*, 79(5):1316-1325, 2011.

69. Dilip, C. S., Venkatachalam, K. J., Raj, A. P., and Ramachandramoorthy, T. Microwave assisted synthesis and structural characterisation of nicotinic acid and nitrito–κO mixed ligand complexes. *Life*, 50:L80-L88, 2011.

70. Chang, J. C., Gerdom, L. E., Baenziger, N. C., and Goff, H. M. Synthesis and molecular structure determination of carboxyl bound nicotinic acid (niacin) complexes of chromium(III). *Inorganic Chemistry*, 22(12):1739-1744, 1983.

71. Do Nascimento, A. L. C. S., Caires, F. J., Gomes, D. J. C., Gigante, A. C., and Ionashiro, M. Thermal behaviour of nicotinic acid, sodium nicotinate and its compounds with some bivalent transition metal ions. *Thermochimica Acta*, 575:212-218, 2014.

72. Soares-Santos, P. C., Paz, F. A. A., Ferreira, R. A. S., Klinowski, J., Carlos, L. D., Trindade, T., and Nogueira, H. I. Coordination modes of pyridine-carboxylic acid derivatives in samarium (III) complexes. *Polyhedron*, 25(12):2471-2482, 2006.

73. Gogoi, S. R., Boruah, J. J., Sengupta, G., Saikia, G., Ahmed, K., Bania, K. K., and Islam, N. S. Peroxoniobium (V)-catalyzed selective oxidation of sulfides with hydrogen peroxide in water: a sustainable approach. *Catalysis Science & Technology*, 5(1):595-610, 2015.

74. Dengel, A. C., Griffith, W. P., Powell, R. D., and Skapski, A. C. X-Ray structure of $K_4[Mo_2O_2(O_2)_4(C_4H_2O_6)]\cdot 4H_2O$, a novel peroxo complex containing a single

tetradentate bridging tartrate. *Journal of the Chemical Society, Chemical Communications*, (7), 555-556, 1986.

75. Lin-Ven D., Colthup N. B., Fateley W. G. and Grasselli J. G., The Handbook of Infrared and Raman Characteristic Frequencies of the Organic Molecules, Academic, London, 1991.

76. Ferraro J. R. and Nakamoto K., *Introductory Raman Spectroscopy*, Academic, London, 1994.

77. Maurya, M. R., and Bharti, N. Synthesis, thermal and spectral studies of oxoperoxo and dioxo complexes of vanadium (V), molybdenum (VI) and tungsten (VI) with 2-(α-hydroxyalkyl/aryl) benzimidazole. *Transition Metal Chemistry*, 24(4):389-393, 1999.

78. Silverstein, R. M., Bassler, G. C., and Morrill, T. C. *Spectrometric Identification of Organic Compounds*, John Wiley and Sons, New York, 5th edition, 1991.

79. Lorgé, F., Wagner, A., and Mioskowski, C. Improved procedure for routine ^{13}C NMR analysis of Merrifield resin bound molecules. *Journal of Combinatorial Chemistry*, 1(1):25-27, 1999.

80. Mohanraj, S. and Ford, W. T. Analysis of cross-linking of poly [(chloromethyl) styrene] by high-resolution carbon-13 NMR spectroscopy. *Macromolecules*, 18(3):351-356, 1985.

81. Kawamoto, K. and Tsujimoto, Y. Effects of the hydroxyl radical and hydrogen peroxide on tooth bleaching. *Journal of Endodontics*, 30(1):45-50, 2004.

82. Kassaee, M. Z., Sayyed-Alangi, S. Z., and Sajjadi-Ghotbabadi, H. Synthesis and reactions of n-methylbenzyl ammonium fluorochromate(VI) on silica gel, a selective and efficient heterogeneous oxidant. *Molecules*, 9(10):825-829, 2004.

83. LeTiran, A., Stables, J. P., and Kohn, H. Functionalized amino acid anticonvulsants: synthesis and pharmacological evaluation of conformationally restricted analogues. *Bioorganic and Medicinal Chemistry*, 9(10):2693-2708, 2001.

84. Zhu, Y., Jang, S. H. A., Tham, Y. H., Algin, O. B., Maguire, J. A., and Hosmane, N. S. An efficient and recyclable catalytic system comprising nano-iridium (0) and a pyridinium salt of nido-carboranyldiphosphine for the synthesis of one-dimensional boronate esters via hydroboration reaction. *Organometallics*, 31(7):2589-2596, 2012.

85. Labra-Vázquez, P., Palma-Contreras, M., Santillan, R., and Farfán, N. Vibrational, structural and electronic study of a pyridinium salt assisted by SXRD studies and DFT calculations. *Journal of Molecular Structure*, 1131:156-162, 2017.

86. Rodante, F., Marrosu, G., and Catalani, G. Thermal analysis of some α-amino acids with similar structures. *Thermochimica Acta*, 194:197-213, 1992.

87. Weiss, I. M., Muth, C., Drumm, R., and Kirchner, H. O. Thermal decomposition of the amino acids glycine, cysteine, aspartic acid, asparagine, glutamic acid, glutamine, arginine and histidine. *BMC Biophysics,* 11(2):1-15, 2018.

88. Jingyan, S., Jie, L., Yun, D., Ling, H., Xi, Y., Zhiyong, W., and Cunxin, W. Investigation of thermal behavior of nicotinic acid. *Journal of thermal analysis and calorimetry*, 93(2):403-409, 2008.

89. Mukherjee, A. and Biswas, M. Thermal characteristics of iron (III), cobalt (II), and copper (II) complexes of dipyridylamine anchored on polystyrene-divinylbenzene copolymer. *Journal of Applied Polymer Science*, 50(9):1485-1492, 1993.

90. Sharma, M., Saikia, G., Ahmed, K., Gogoi, S. R., Puranik, V. G., and Islam, N. S. Vanadium-based polyoxometalate complex as a new and efficient catalyst for phenol hydroxylation under mild conditions. *New Journal of Chemistry*, 42(7):5142-5152, 2018.

91. Parida, K.M., Sahoo, M., and Singha, S. A novel approach towards solvent-free epoxidation of cyclohexene by Ti (IV)–Schiff base complex-intercalated LDH using H_2O_2 as oxidant. *Journal of Catalysis*, 276(1):161-169, 2010.

92. Sharpless, K. B., Townsend, J. M., and Williams, D. R. Mechanism of epoxidation of olefins by covalent peroxides of molybdenum(VI). *Journal of the American Chemical Society*, 94(1):295-296, 1972.

93. Rösch, N., Gisdakis, P., Yudanov, I. V., and Di Valentin, C. Mechanistic Aspects of Transition Metal-Catalyzed Olefin Epoxidation from Density Functional Studies. In Adam, W., editor, *Peroxide Chemistry: Mechanistic and Preparative Aspects of Oxygen Transfer*, pages 601-619. Wiley-VCH, Weinheim, 2000.

94. Yudanov, I. V. Mechanism of olefin epoxidation with transition metal peroxo complexes: DFT study. *Journal of Structural Chemistry*, 48(1):S111-S124, 2007.

95. Deubel, D. V., Frenking, G., Gisdakis, P., Herrmann, W. A., Rösch, N., and Sundermeyer, J. Olefin Epoxidation with Inorganic Peroxides. Solutions to four long-standing controversies on the mechanism of oxygen transfer. *Accounts of Chemical Research*, 37(9):645-652, 2004.

96. Gisdakis, P., Yudanov, I. V., and Rösch, N. Olefin epoxidation by molybdenum and rhenium peroxo and hydroperoxo compounds: A density functional study of energetics and mechanisms. *Inorganic Chemistry*, 40(15):3755-3765, 2001.

97. Herbert, M., Montilla, F., and Galindo, A. Olefin epoxidation in solventless conditions and apolar media catalysed by specialised oxodiperoxomolybdenum complexes. *Journal of Molecular Catalysis A: Chemical*, 338(1-2):111-120, 2011.

98. Ghiron, A. F. and Thompson, R. C. Comparative kinetic study of oxygen atom transfer reactions of oxohydroxodiperoxomolybdenum(VI) and oxo (oxalato) diperoxomolybdenum(VI) in aqueous solution. *Inorganic Chemistry*, 28(19):3647-3650, 1989.

99. Reynolds, M. S., Morandi, S. J., Raebiger, J. W., Melican, S. P., and Smith, S. P. Kinetics of bromide oxidation by (oxalato) oxodiperoxomolybdate(VI). *Inorganic Chemistry*, 33(22):4977-4984, 1994.

100. Sensato, F. R., Custodio, R., Longo, E., Safont, V. S., and Andres, J. Sulfide and sulfoxide oxidations by mono-and diperoxo complexes of molybdenum. A density functional study. *The Journal of Organic Chemistry*, 68(15):5870-5874, 2003.

101. Djordjevic, C., Vuletic, N., and Sinn, E. Synthesis and properties of peroxo α-amino acid complexes of molybdenum (VI). The structures of $MoO(O_2)_2(HAA)(H_2O)$, HAA= glycine, proline. *Inorganica Chimica Acta*, 104(1):L7-L9, 1985.

102. Gharah, N., Chakraborty, S., Mukherjee, A. K., and Bhattacharyya, R. Oxoperoxo molybdenum(VI)-and tungsten(VI) complexes with 1-(2′-hydroxyphenyl) ethanone oxime: Synthesis, structure and catalytic uses in the oxidation of olefins, alcohols, sulfides and amines using H_2O_2 as a terminal oxidant. *Inorganica Chimica Acta*, 362(4):1089-1100, 2009.

103. Zare, M. and Moradi-Shoeili, Z. Oxidation of alkenes catalysed by molybdenum (VI)–oxodiperoxo complex anchored on the surface of magnetic nanoparticles under solvent-free conditions. *Applied Organometallic Chemistry*, 31(6):e3611, 2017.

104. Cvijanović, D., Pisk, J., Pavlović, G., Šišak-Jung, D., Matković-Čalogović, D., Cindrić, M., Agustin, D. and Vrdoljak, V. Discrete mononuclear and dinuclear compounds containing a MoO_2^{2+} core and 4-aminobenzhydrazone ligands: synthesis, structure and organic-solvent-free epoxidation activity. *New Journal of Chemistry*, 43(4):1791-1802, 2019.

105. Coelho, A. C., Balula, S. S., Bruno, S. M., Alonso, J. C., Bion, N., Ferreira, P., Pillinger, M., Valente, A. A., Rocha, J. and Gonçalves, I. S. Grafting of Molecularly Ordered Mesoporous Phenylene-Silica with Molybdenum Carbonyl Complexes: Efficient Heterogeneous Catalysts for the Epoxidation of Olefins. *Advanced Synthesis & Catalysis*, 352(10):1759-1769, 2010.